Durham E-Theses

GEOCHEMICAL CONSTRAINTS ON HISTIDINE ADSORPTION BY LAYERED DOUBLE HYDROXIDES

LEE, DUAN-CHERN

GEOCHEMICAL CONSTRAINTS ON

HISTIDINE ADSORPTION BY

LAYERED DOUBLE HYDROXIDES

Duan-Chern Lee

Thesis Prepared for the Degree of

Master of Science

Department of Chemistry

Durham University

October, 2012

Abstract

Duan-Chern Lee, Geochemical Constraints on Histidine Adsorption by Layered Double Hydroxides.

To unravel the mystery of how life may have emerged on the early Earth, the last century has, increasingly, seen concerted attempts to investigate the environmental conditions and potential chemistry present. As more hypotheses have been tested, many researchers now believe that it is the hydrothermal vents under the ancient ocean that would have provided the environment and the starting materials ready for the reactions to create life.

Layered clay minerals would also most likely have played a significant role in these prebiotic reactions. These minerals would have concentrated the starting materials for life's chemistry through intercalation, catalysed the reactions that formed biomolecules, and protected the resulting products from decomposition, in a sense the same processes as life carries out today, but in different ways.

In this study, the layered hydroxide mineral $Mg_2Al(OH)_6Cl \cdot zH_2O$ was used to mimic the green rust, $Fe^{II}_2Fe^{III}(OH)_6A^{n-}_{1/n} \cdot yH_2O$, a mineral that could have been one of the most-common components of early ocean sediments but is also highly redox reactive, in the intercalation reaction of histidine, one of the amino acids essential in modern day biochemistry. A co-precipitation method was used in the preparation of the Mg_2Al-Cl LDH, which was later used in the ion-exchange reactions with D, L-histidine solution at different pH (7 and 10), temperature (30 °C and 60 °C), and pressure (ambient and ~ 50 bar). Among all the potential environmental conditions tested, the reaction at pH 10, 30 °C showed the highest ion-exchange rate. There was also a small (less than 2 % in exchanging rates) chiral selectivity observed in all reactions, but no correlation in trends between different conditions could be drawn.

Table of Contents

List of Tables

List of Figures

x

Acknowledgements

1. Introduction

1.1 Literature Review

1.1.1 Introduction

Life is difficult to formally define, though can be stated to include seven aspects[1]: the ability to regenerate by genetic information; the ability to adapt through natural selection; compartmentalisation of structures to reach concentrations sufficient for reactions to occur; metabolic pathways to get source of energy and discard waste; regeneration from the wear and tear of the system; feedback mechanisms for short-term environmental change; seclusion of reactions to select the specific reactions in life. There is a more conclusive definition of life from Oliver and Perry[2]:

"*Life is the sum total of events which allows an autonomous system to*

respond to external and internal changes and to renew itself from which

in such a way as to promote its own continuation."

The origin of life remains one of the most significant questions left to humankind, and is also one of the most challenging research areas. From the evidence left on modern Earth, many different paths to unravel this process have already been tried, however there are still many difficulties arising when trying to rationalise how life emerged on ancient Earth. Among all approaches tried, the geochemical approach has unravelled most about the environment of the prebiotic world, with the starting materials ready for the reactions to create life.

1.1.2 Early Earth Chemistry

1.1.2.1 Environment on the Early Earth

Life emerged approximately 3.8 billion years ago,[3] a time that only limited evidence about the environment can be left until today. Beyond the exogenesis theory that life is formed by extraterrestrial sources, there are two principle endogenesis theories of how life began:

1. Primordial soup: The environment of the early Earth was very harsh for organisms, with the atmosphere containing only methane, hydrogen, ammonia and water vapour.[4, 5] Between the components in the oceans and the atmosphere, the reactions occur using energy supplied from various sources, such as ultraviolet (UV) radiation.[4, 6]

2. Oceanic hydrothermal vents: Prebiotic reactions occur in the ocean where the submarine volcanoes were venting hot, chemical rich fluids.[7] Chemical energy is derived from reduction-oxidation (redox) reactions of hydrogen molecules with those of carbon dioxide or carbon monoxide.

The hypothesis of a "primordial soup" was proposed earlier, in the mid-20th Century, following the key results of the "Miller-Urey experiment", 11 out of 20 amino acids (more recently, 22 amino acids were found when the sealed product from the original experiment was re-analysed)[8] that make up proteins in living cells were formed in various concentrations after the lightening-simulating sparks were fired in a gas mixture of water (H_2O), methane (CH_4), ammonia (NH_3), and hydrogen (H_2).[9, 10]

However, it has been subsequently proposed that the conditions on the primitive Earth were not likely as originally proposed in this theory. In contrast, researchers now think that the atmosphere was mainly composed of carbon dioxide (CO_2), water vapour (H_2O), and nitrogen (N_2) with minor amounts of carbon monoxide (CO), hydrogen (H_2), methane (CH_4), sulfur dioxide (SO_2) and oxygen (O_2).[11] Moreover, one of the major energy source in this hypothesis, UV light, is also known to destroy these small organic molecules of the type that had already been produced.[12] Given this, the theory of life arising at hydrothermal vents seems to have become more dominant, perhaps due to being more viewed as more plausible.

1.1.2.2 *Building Blocks of Biomolecules*

Once simple organic molecules were formed and concentrated, large biomolecules had to be formed in order for the functioning of the first proto-cells. One of the very central functions is the ability to carry, and to pass on, information by replication, and this can only be done by two main types of biomolecules, proteins and nucleic acids.[5] Since this task is done by nucleic acids in the modern world, Thomas R. Cech,[13, 14] Sidney Altman[15, 16] and Gerald F. Joyce[17, 18] believe that nucleic acids were produced on the early Earth and played this important role first, just as they do today. There is, however, some evidence supporting the fact that the proteins or peptides became the first to be the key to replication, and were later substituted by nucleic acids. These hypotheses are known as the "RNA World"[19] and "Peptide World",[5, 20] respectively.

Although these ideas simplify the problem of catalysis and the evolution of information, the theory of an "RNA World" has some major flaws. Nucleic acids are unstable in the presence of high intensity UV radiation as encountered in the prebiotic

world. Ribose and nucleobases also have short half-lives, since nucleophilic attack would easily cause phosphoester-bond damage and hydrolysis.[5]

The lack of repair mechanisms is another reason that challenges the idea of the "RNA World". Even the smallest mutation on a nucleic acid sequence can bring about large changes in genetic information and hence, the greatest damage to proto-life. In contrast, the errors that occur in a peptide sequence are less damaging, since the properties of a whole peptide do not alter dramatically with a change of a single amino acid.

One of the tertiary structures of peptides, based on a β-sheet secondary conformation, may offer a way to avoid decomposition of early genetic materials in an early Earth environment. Known as an amyloid, these structures have been proposed to meet the conditions for the formation of life: the ability to replicate, evolve and increase in complexity, and all in extreme conditions.[20]

In this study, the hypothesis of the "Peptide World" is focussed on, and nucleic acids are considered to have been left for later development as a more mature system.

1.1.3 Amino Acids and Peptide Formation

Amino acids serve as the building blocks of peptides and polypeptides, with the latter also known as proteins, which, together with polysaccharides and nucleic acids, are the essential biological macromolecules in organisms. It is this reason that makes the formation of peptides the key to the formation and hence the origin of life.

1.1.3.1 Protein Structure

There are four distinct levels of protein structure. The primary structure of a

protein determines its secondary, tertiary, and quaternary structures.

The primary structure of a protein is the sequence of amino acids in the polypeptide chain. Each amino acid is covalently bonded to the next one with an amide bond between the carbonyl group of one amino acid and the amine of another, forming the backbone of the peptide chain. Usually, the primary structure is described using the three-letter abbreviations of the amino acids in sequence, starting from the residue of the free-amino end (N-terminus) to the residue of the free-carboxylate end (C-terminus).

There are two main types of highly regular secondary sub-structure, α-helix and β-sheet, and their conformations are constrained by hydrogen bonds. In the α-helix structure, the polypeptide chain right-handedly spirals up, and each amino acid residue forms hydrogen bonds with the adjacent ones, using an upward amino group and downward carbonyl group. On the other hand, in the β-sheet structure, the polypeptide chain is arranged anti-parallel to the adjacent chain, and hydrogen bonds are formed between each of the adjacent amino acid residues.

The tertiary structure is a three dimensional structure of a single polypeptide chain. The tertiary structure is stabilised by various interactions between the R-groups of amino acid residues, including ionic bonds between charged R-groups, hydrogen bonds between R-groups with hydrogen bond donors and acceptors, "sulfur bridge" between the oxidised thiol groups of two cysteines, and van der Waals dispersion forces between hydrophobic R-groups.

The quaternary structure refers to the three-dimensional structure composed of multiple polypeptide molecules, or so-called "monomers". The most common example used to illustrate quaternary structure is the protein hemoglobin (**Figure 1**). There are four monomers in hemoglobin: two α-chains, each with 141 amino acids,

and two β-chains, each with 146 amino acids.

(A)

± Lys ± Ala ± His ± Gly ± Lys ± Lys ± Val ± Leu ± Gly - Ala ±

(B)

(C)

(D)
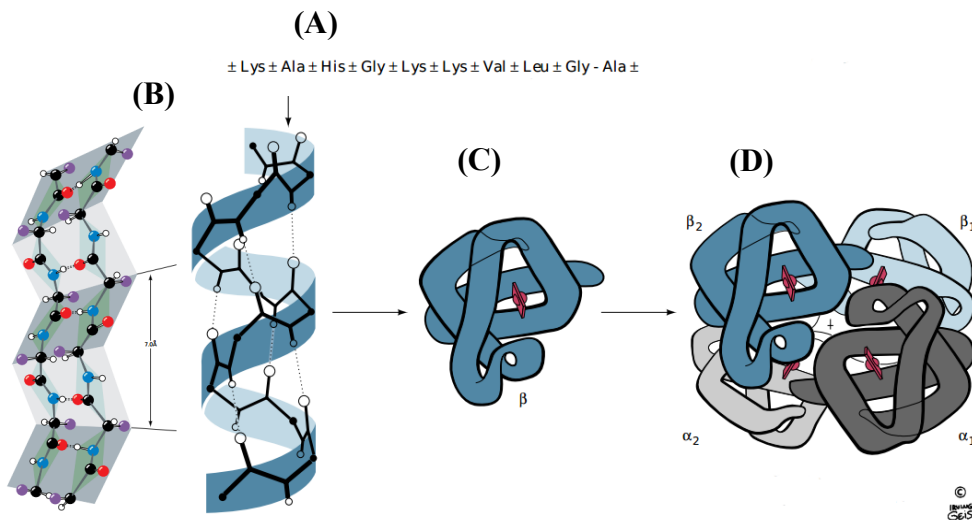
Figure 1   **(A)** Primary structure: amino acid sequence, **(B)** secondary structure: α-helix (right) and β-sheet (left), **(C)** tertiary structure: β-chain of hemoglobin, and **(D)** quaternary structure: four separate polypeptide chains assembled into the hemoglobin (modified from Voet *et. al.*)[21].

1.1.3.2   *Peptide Forming Reactions*

Peptide formation is a second order, concentration dependent reaction, whereas the hydrolysis (the reverse reaction) is a pseudo first order reaction, which is mainly concentration independent.[22]

Thermodynamically, the overall reaction is unfavourable for peptide formation to occur in solution, with a small, positive value of ΔG° (see **Figure 2** below). This is not surprising since the dehydration, simultaneously proceeding with peptide formation, must be difficult in the presence of water as the solvent. Kinetically, each pathway contains a strained 4-membered ring as a transition state which precedes proton transfer, leading to a high-energy barrier that slows down the reaction.[24]
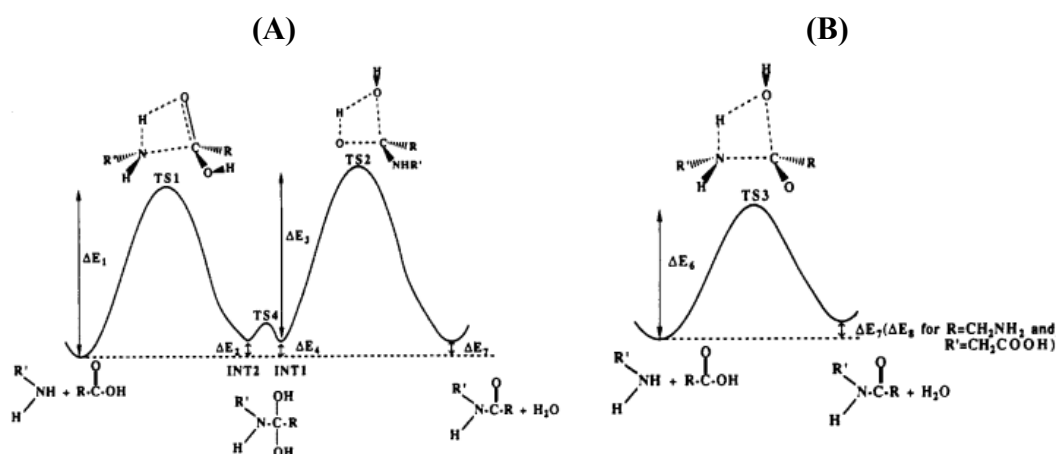
Figure 2 Peptide forming reaction via **(A)** a stepwise mechanism and **(B)** a concerted mechanism (taken from Jensen *et al.*, 1992).[23]

To improve this reaction, the thermodynamics must be adjusted to favour the peptide bond formation before considering speeding up the rate of reaction. There are various mechanisms that have been proposed in order to fit the situation on the prebiotic Earth: by removing the produced water, the reaction is driven in the direction of the condensation product through Le Chatelier's Principle; i.e. via the dry state reaction,[25] or by drying and wetting cycles,[26] which have been reported to mimic the conditions of coastal areas or lagoon environments.[27] Also, the use of condensation reagents, such as carbonyl sulfide,[28] which raises the energy of starting materials, can also drive the reaction to completion. Another hypothesis, called "Salt Induced Peptide Formation" (SIPF), is introduced here.

1.1.3.3 Salt Induced Peptide Formation (SIPF)

Reported by Schwendinger and Rode in 1989,[29] salt induced peptide formation

7

uses Cu^{2+} as catalyst and NaCl as dehydrating agent. It proceeds through a monochlorocuprate intermediate, where the copper ion is bound by a bidentate and a monodentate amino acid.
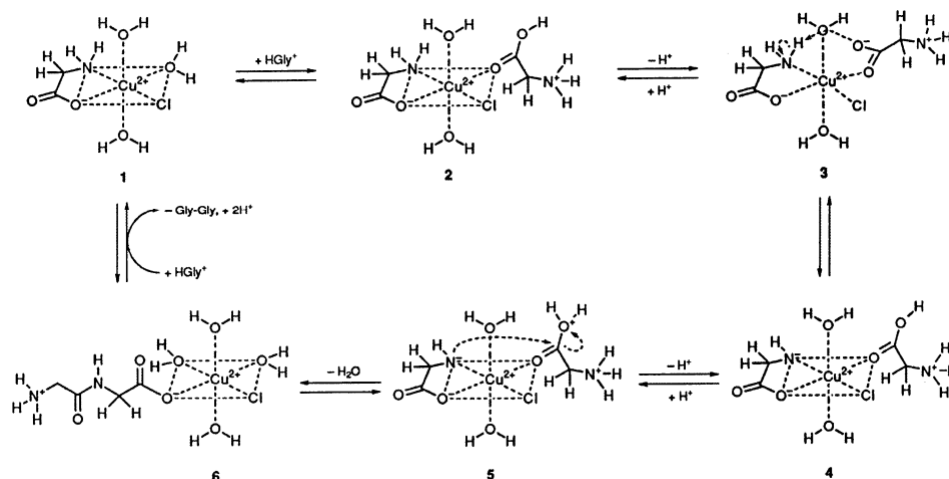
Figure 3   Salt induced peptide formation from copper-glycine complex by Schwendinger and Rode (take from Rode and Suwannachot, 1999).[30]

Rode *et al.* have reported that all amino acids thus far experimented on have been successfully polymerised to form dipeptides, and, with the presence of mineral catalysts, the formation of peptides would be favoured to go further, forming oligopeptides up to hexamers.[26]   Further studies have highlighted the similarity between the sequences of the peptides produced from SIPF and the membrane proteins in prokaryotes, which would have been the first cellular organisms to exist on the early Earth.[26] The above research strongly suggests that SIPF reactions may have been operating in the prebiotic oceans. All of which provides evidence of SIPF as having occurred in the prebiotic world.

1.1.3.4 Mineral Mediated Peptide Formation

There are still limits to SIPF, where a wetting and drying environment is required. Peptide formation in clay minerals is one of the postulated conditions for this process on the prebiotic Earth.

Clay minerals are hydrated aluminium phyllosilicates, consisting of two-dimensional inorganic layers, sometimes with variable amounts of iron, magnesium, alkali metals, alkaline earths and other cations. They are composed of linked tetrahedral and octahedral sheets, with the ratio 1:1 or 1:2.
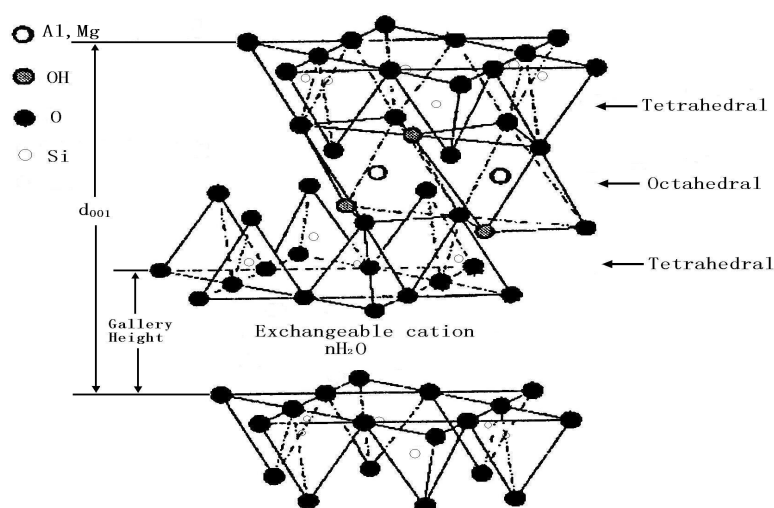
Figure 4   Structure of smectite, one of the clay minerals (from Chen *et al.*).[31]

With the silicons replaced by aluminium, the negatively charged layers require positively charged ions to charge balance within the interlayers. Through adsorption of amino acid zwitterions, polymerisation to peptides can occur, catalysed by either the clay itself or by Cu^{2+} charge balancing cations through SIPF. The interlayer of clay provides not only the host to concentrate amino acids, but also shelter to protect the condensed peptide from subsequent hydrolysis by inclusion within the interlayers.[32]

1.1.4 Layered Double Hydroxides

Green rust, a Fe^{II}/Fe^{III} mineral that is thought to have been one of the most-common components of early ocean sediments,[32] is a layered double hydroxide (LDH), which are a group of natural and synthetic minerals that share a similar structure with that of brucite, $Mg(OH)_2$. In brucite, magnesium cations form a closed-pack layer and hydroxides are coordinated above and below the metal layer with the oxygen-hydrogen bonds perpendicular to the metal plane. Each metal cation is directly bonded to six hydroxide groups, and each hydroxide group is directly bonded to three metal ions. These two-dimensional sheets then layer to form three-dimensional crystals of brucite. In the main type of LDHs, on the other hand, the magnesium layer is substituted with a mixed-metal layer, with both divalent and trivalent cations. Since the trivalent cations introduce net positive charges in the hydroxide layers, the counterions are anionic and again situated between layers for charge balance.
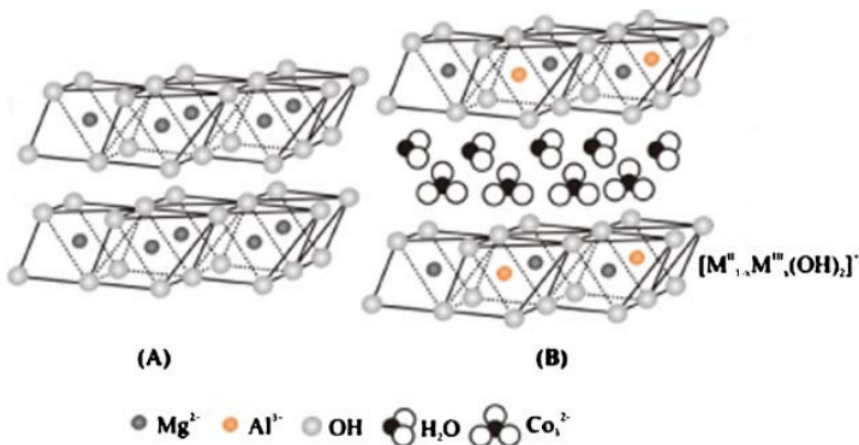
Figure 5   Schematic representation comparing the crystal structure of **(A)** brucite and **(B)** LDH (taken from Costa *et al.*, 2008).[34]

10

The general formula for the majority of LDHs is:

$$[M^{2+}_{1-x}M^{3+}_{x}(OH)_2]^{x+}[A^{n-}]_{x/n} \cdot yH_2O \qquad \textbf{Formula 1}$$
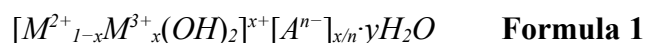
where x usually falls in the range of 0.2 ~ 0.33,[35] i.e. the ratio of divalent to trivalent cations is typically between 4:1 to 2:1. The values of counterion A depend on the charge of the anion and the amount of trivalent metal, so that the x/n achieves charge neutrality throughout the LDH structure. There are also water molecules in the interlayer, forming hydrogen bonds to the hydroxyl groups on the layer.[36] An example of the formula is $Mg_6Al_2(OH)_{16}CO_3 \cdot 2H_2O$, which belongs to hydrotalcite, the most common naturally occurring LDH.

Layered double hydroxides are often referred to as anionic clays. Unlike usual clay minerals that have negative-charged layer and positive-charged interlayer, LDHs are formed with positive-charged layer, and the exchangeable interlayer ions are negatively-charged. Therefore, LDHs are utilised as anion exchanging materials.[37, 38, 39] In fact, the preference of anions by LDHs has already been investigated in the 1970s – 1980s for this purpose.[40, 41] In these studies, carbonate, among the simple inorganic and organic anions, is the easiest to intercalate and the hardest to exchange from within the LDHs. On the opposite end, halides and nitrate are the easiest to exchange. As a result, chloride or nitrate are often used as the interlayer anion in LDH as starting materials and then exchanged with the desired anions.

Electro-photoactive materials,[42] drug-delivery systems,[43, 44] adsorbents,[45] and flame retardants[46, 47] are some other practical uses of LDHs. In this project we propose to use LDHs for the synthesis of peptides in simulated prebiotic

environments. In alkaline hydrothermal conditions, amino acids, bearing net negative charges, are able to intercalate into catalytic LDHs.

Instead of using green rust itself in this study, the Mg^{II}/Al^{III} LDHs are used since they are isostructual with the Fe^{II}/Fe^{III} LDHs, but are advantageous in that they are not prone to rapid oxidation. However, a key difference is that in Fe^{II}/Fe^{III} system, charge migration between Fe^{II} and Fe^{III} can occur.[48] Related research by Hibino[49] showed that 14 out of 20 proteinogenic amino acids were able to intercalate into Mg/Al-LDH by co-precipitation synthesis with Mg:Al set at 3:1, and the charge occupation rates by histidine in different preparation conditions were 18.0 % and 26.5 %.

1.1.5 Homochirality

Homochirality describes the property of certain molecules to occur in two forms that are non-superimposable mirror images of one another. The symmetry is usually introduced around a chiral centre, such as a carbon atom with four different substituents.

The origin of homochirality is said to evolve in three steps: mirror-symmetry breaking introduces the enantiomeric imbalance and is the most dominant step; chiral amplification is the process of enantiomeric enrichment; and the third step, chiral transmission, allows the transfer of one chiral form to another.[50]

The majority of amino acids that assemble biological proteins on present day Earth are in the L-configuration. Use of the other enantiomer can lead to structural changes in biomolecules and lead to changes in, or cessation of, correct function. However, more than 70 chiral amino acids, biological and non-biological, found in

meteorites were racemic,[51] with only the one exception of isovaline, an amino acid that is too rare on Earth to have been introduced via terrestrial contamination, from the Murchison meteorite.[52] This means that, at an early point in the origin of life, symmetry-breaking, the move from racemic mixtures of both enantiomers to homochirality, was introduced and then so was enantiomeric enrichment in order to meet the conditions found in modern Earth.[53]

A suggested route to symmetry-breaking is via circular-polarised light, reported by Shibata *et al.*, in 1998.[54] Another speculated pathway suggests that β-decay leads to slightly different half-lives of biologically relevant molecules.[55] Clay minerals are also another possible key factor in this important step.[55]

Some clays select specific enantiomers preferentially, either through thermodynamic or kinetic routes. From thermodynamic data, the homo-diastereomer of dialanine (Ala$_2$), D-Ala-D-Ala or L-Ala-L-Ala, is reported to show selective adsorption on certain clays, since the homo-diastereomeric molecules were stabilised by the mineral surface, whilst the hetero-diastereomers, D-Ala-L-Ala and L-Ala-D-Ala, were more stable in solution.[53] Kinetic routes involve differences occurring in the rate of intercalation-deintercalation of enantiomers, and differences between D- and L-histidine intercalation in LDH minerals have been reported by Ikeda *et al.*.[56] Once the preferential selected enantiomer is adsorbed on the clay mineral, it is protected from racemisation that might occur under the extreme conditions on the prebiotic Earth, and therefore, amplified to reach homochirality.[57, 58]

Asymmetric catalysis is the other pathway to symmetry-breaking. In salt induced peptide formation reactions, the geometry of the copper complex leads to the preference of reaction of L-amino acids.[59]

1.2 Introduction and Objectives

Geochemistry, as a precursor of biochemistry, played a significant role in terms of the conditions that existed for proto-biological chemistry to occur on the prebiotic world. Before biochemical catalysts, nucleic acids and proteins must have arisen through abiotic processes, and evolved in the early world to function as today.

The aims of this present study are:

- To prepare a mineral analogous to those that may have formed on early Earth hydrothermal seeps, a layered double hydroxide with chloride as the readily exchanged anion (LDH-Cl), by a co-precipitation method.

- To ascertain the geochemical constraints (the effects of pH value, temperature, and pressure) on the intercalation of a representative amino acid, histidine, in order to determine the most likely environments that early peptides may have evolved.

- To determine whether chiral selectivity occurs during adsorption of amino acids within the LDH-Cl mineral.

2. Experimental Methods

2.1 Materials

Sodium chloride was obtained from the Department of Chemistry, Durham University, store, whilst the other inorganic salts and histidine were purchased from Sigma-Aldrich in analytical grade quality. The perchloric acid for high performance liquid chromatography (HPLC) was purchased from Sigma-Aldrich, and the other eluents were obtained from the HPLC laboratory as HPLC grade. All these substances were used without further purification.

2.2 Preparation of Layered Double Hydroxide Mineral

The co-precipitation method[60] was used to prepared the LDHs, and N_2 was used to avoid the intercalation of carbonate anion ($CO_3^{2-}_{(aq)}$), from solution capture of $CO_{2(g)}$ in the air, into the interlayer of LDH under the pH 10 synthesis conditions. Instead of Fe^{2+}/Fe^{3+} in green rust, Mg^{2+}/Al^{3+} were used as the cations in host layers to prevent structure change through oxidation of Fe^{2+}.[33]

$AlCl_3 \cdot 6H_2O_{(s)}$ (5.66 g, 23.46 mmol) and $MgCl_2 \cdot 6H_2O_{(s)}$ (9.54 g, 46.92 mmol) were dissolved in 100 mL deionised water. A solution of $NaCl_{(s)}$ (6.855 g, 117.3 mmol) in 100 mL deionised water was stirred and heated at 60 °C with a $N_{2(g)}$ flow blanketing the whole system. The metal chloride solution was then added drop-wise, whilst a 100 mL solution of $NaOH_{(s)}$ (10 g, 250 mmol) was simultaneously added to maintain the system at a constant pH of 10. Once the metal chloride solution was completely added, the solution was left to react for 24 hours before being filtered under $N_{2(g)}$ and washed with 1 L of 60 °C deionised water. The recovered precipitate

was then dried in an oven at 80 °C for 24 hours before being finely ground with an agate mortar and a pestle. The produced powder was stored in a vial.

2.3   Adsorption Experiments

2.3.1   The Effects of pH and Temperature on Adsorption

A multi-flask reactor heated at a set temperature was used with a gas flow of nitrogen ($N_{2(g)}$) circulation to avoid dominant adsorption of carbonate over histidine. Six different concentrations of D, L-histidine$_{(aq)}$ were prepared in deionised water and 50 mL volumetric flasks, and transferred to the two-neck flasks. 250 mg of LDH was then added to each flask. After 24 hours reaction, the solution in each flask was taken out by a syringe with needle and directly filtered with a 0.22 μm microporous membrane from Millipore into a marked vial. The reacted LDH was then filtered and washed with 50 mL deionised water, before being dried in the oven at 80 °C.

Concentration (M)	0.08 M histidine$_{(aq)}$ (mL)	1 M NaOH$_{(aq)}$ (mL)
0.06	37.5	2.01
0.04	25	1.34
0.02	12.5	0.67
0.01	6.25	0.34
0.006	3.75	0.27
0.004	2.5	0.14

Table 1 The calculated amounts of histidine and sodium hydroxide solution that are needed to prepare 50 mL histidine at pH 10.

To prepare D, L-histidine$_{(aq)}$ for pH 10 experiments, the D, L-histidine$_{(aq)}$

solution was diluted using 1 M $NaOH_{(aq)}$ and deionised water in a 50 mL volumetric flask. A calibrated pH probe was used to measure the pH.

Since $N_{2(g)}$ flow was circulating through the whole reactor, evaporation of some solution was inevitable during the 24-hour adsorption at higher temperature. Hence, these solutions would have become more concentrated over time and a source of potential error was introduced. Owing to this, the reactions were re-run where the side-necks of flasks were sealed by glass plugs, or rubber stoppers, after the solution and LDH were added over 20 minutes of $N_{2(g)}$ circulation. Circulating water was also used in the reflux cooling block on the reactor system to condense any evaporated solvent. The reactor was then heated up to the assigned temperature for reaction, thus minimising any water loss issues.

2.3.2 The Effect of Pressure on Adsorption

A HEL Cat-7 high-pressure reactor with seven vials was used at set pressure and temperature. 50 mg of LDH and a stirrer bar were first placed in each number-marked vial. A glove bag with nitrogen purge was then used to prevent any contamination of the reactor with $CO_{2(g)}$ during the preparation of the solutions. 0.08 M D, L-histidine$_{(aq)}$ (0.6202 g, 4 mmol) was made in a 50 mL volumetric flask after the pH was adjusted to 10 by addition of 1 M $NaOH_{(aq)}$. A solution of 100 mL, pH 10 water was also prepared with deionised water and 1 M $NaOH_{(aq)}$. By varying the ratios of the two solutions described above, seven different concentrations of 10 mL, pH 10 D, L-histidine$_{(aq)}$ were able to be prepared, *in situ*, in the reactor vials, before being sealed with parafilm. The high-pressure reactors were then set up, with a chiller unit circulating the cooling head to prevent fluid transfer, at a calculated,

pre-set pressure for later heating up to the desired temperature and pressure. Solutions were taken out by a syringe with needle and directly filtered with the 0.22 μm micro-porous membrane and analysed by chiral HPLC after each 24-hour reaction.

Vial No.	Concentration (M)	0.08 M histidine$_{(aq)}$ (mL)	Water at pH 10 (mL)
1	0.08	10	0
2	0.06	7.5	2.5
3	0.04	5	5
4	0.02	2.5	7.5
5	0.01	1.25	8.75
6	0.008	1	9
7	0.004	0.5	9.5

Table 2 The amounts of histidine and water previously adjusted to pH 10 that are needed to prepare 10 mL histidine solution.

2.4 *Analytical Methods*

Various analytical methods were used to gain detailed information from the two major products of the experiments: layered double hydroxide (chloride and amino acid exchanged) powder and histidine solutions.

2.4.1 Elemental Analysis (CHN)

The elemental analysis for carbon, hydrogen and nitrogen was accomplished by combustion analysis. A sample was weighed before being combusted under high-temperature in an oxygen environment. The gas products were processed for

removal of excess oxygen and other interferences to obtain a homogeneous mixture of carbon dioxide (CO_2), water (H_2O) and nitrogen (N_2). The gas stream then passed through a carbon dioxide trap and a water trap sequentially, and the compositions of elements C, H and N in the sample were determined.

For synthetic LDHs in this study, there was no nitrogen introduced during co-precipitation, hence, the amount of adsorbed amino acid during adsorption could be calculated with the %N. On the other hand, the %C and the %H could be used to determine the amount of carbonate and water in the original chloride LDHs.

An Exeter Analytical Inc. Elemental Analyser CE440 was used for carbon, hydrogen and nitrogen elemental analysis.

2.4.2 Mass Spectrometry (MS)

Mass spectrometry separates and detects ions or molecules based on their mass-to-charge ratios. It consists of three main parts: an ion source which converts the ions or molecules in the sample to gas-phase charged particles, a mass analyser which sorts the ions by applying an electromagnetic field when the ions pass through, and a detector which measures the quantity of sorted ions. There are both qualitative and quantitative uses of this technique, such as identifying unknown compounds (owing to extreme sensitivity), determining the isotopic composition of elements in molecules, and quantifying the amount of compounds in a sample.

Mass spectrometry works not only as an analytical method, but also sometimes as a detector used in line on other instruments. These include gas chromatography (GC), liquid chromatography (LC), inductively coupled plasma (ICP), and even with another mass spectrometer. In this study, mass spectrometry

was coupled with a thermogravimetric analyser (TGA), a technique which is introduced below.

2.4.3 Thermogravimetric Analysis (TGA)

This technique involves heating up the target sample at a constant rate whilst measuring the weight loss. During the analysis, weight loss may occur due to several processes such as desorption, dehydration or decomposition. Other processes, such as oxidation of any residual ash, may contribute to the weight gain. Coupled with a mass spectrometer, the molecules that evaporate, or form through decomposition reactions, during heating can be characterised, and thus the structure of the material can be determined.

From LDH samples, the intention would be to look for H_2O, CO_2 and HCl lost from the interlayer water, chloride or any carbonate contamination before de-hydroxylation of the hydroxide layers. From histidine-adsorbed LDHs, NO_x from decomposition of amino acids would also be potentially identified.

TGA was performed on a Perkin Elmer Pyris 1, coupled with a Hiden Analytical Ltd. HPR 20 mass spectrometer. The sample was heated from room temperature to 1000 °C at a rate of 10 °C/min and purged with helium through to a mass spectrometer for analysis.

2.4.4 Inductively Coupled Plasma Optical Emission Spectrometry (ICP-OES)

This technique uses the inductively coupled plasma (ICP) to produce

sample-originated, excited atoms or ions that emitted electromagnetic radiation at characteristic wavelengths, with which the elements within the sample can be identified. Additionally, the concentrations of the elements in the sample can be calculated from the intensities of the emissions.

Essentially, ICP consists of three concentric quartz tubes and two coils. There is argon flow in the outer tube, which is ionised by a Tesla coil to create a plasma. The plasma is then enhanced by the second coil, which is connected to a high-power radio frequency generator. This high temperature plasma breaks down all the molecules from the sample into atomic ions, and rapid recombination of ions and electrons emit electromagnetic radiation, which is then detected by a spectrometer.

In this study, ICP-OES was used to determine the amount of magnesium and aluminium in the LDHs. Combined with the information from the elemental analysis, the composition and the ideal adsorption capacity of LDHs were calculated.

ICP-OES was performed on a Horiba Scientific ULTIMA 2, after dissolving the LDH samples in nitric acid.

2.4.5 Powder X-Ray Diffraction (PXRD)

X-ray diffraction is one of the most frequently used techniques for obtaining detailed information about the crystal structure of organic and inorganic materials with long-range order. With use of angstrom-wavelength range X-rays, arrays of atoms (which are also in a similar size range) in the crystals can be used as a diffraction grating to scatter a monochromatic beam of X-rays. The scattered X-rays then produce either constructive or destructive interference depending on whether they satisfy Bragg's Law or not:

$$\lambda = 2d_{hkl}\,sin\,\theta \qquad \textbf{Equation 1}$$

Where d_{hkl} is the distance between two adjacent parallel planes with their Miller Indices being (*hkl*) and θ is the Bragg's angle between the incident and diffracted beam.

Single crystal X-ray diffraction is extremely powerful for mono-crystalline solids, but for synthesised LDHs a single crystal sample is usually unachievable, with sample being polycrystalline, consisting mainly of crystals in the sub-200 nm size range. Therefore, powder X-ray diffraction (PXRD) is used here for structure analysis. The powder sample is placed on the sample holder and the X-ray beam and detector are rotated through 2θ angle between $2° − 80°$. The intensity of every direction in this range is then calculated through the beam collected by the detector, and the graph that shows us the diffraction pattern is produced.

Though LDHs are rather disordered, there is still key information we can obtain from the XRD pattern. The two most relevant items of data are the *a* parameter and the *c* parameter. The former can be used to determine the M^{2+}/M^{3+} ratio, whilst the latter can be used to calculate the gallery height (the space between the mineral sheets), with the aid of information that the hydroxide layer is about 2.7 Å in height and the hydrogen bonding space is about 2.1 Å:[61]

$$\text{gallery height (Å)} = \text{d-spacing} − (2.7 \text{ Å} + 2.1 \text{ Å}) \qquad \textbf{Equation 2}$$
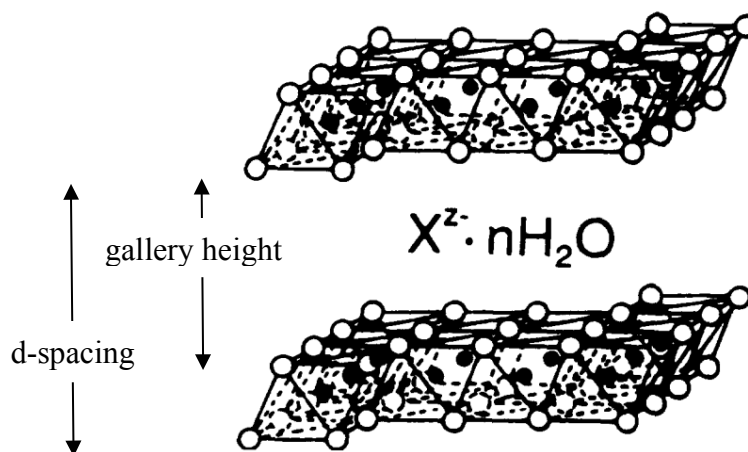
Figure 6   LDH framework, $[Mg_{1-x}^{2+}Al_x^{3+}(OH)_2]^{x+}(X^{z-})_{x/z}.nH_2O$, where $\bullet = Mg^{2+}$ or

Al^{3+} and $\circ$ = hydroxyl group (taken from Porta, 1995)[62]

Both a Siemens Diffractometer D5000 and Bruker D8000 Advance were used to obtain XRD data of LDHs, with use of Cu K_α radiation and 2θ angle ranging from $2° - 80°$.

2.4.6 High Performance Liquid Chromatography (HPLC)

HPLC is a chromatographic technique that can separate a mixture of compounds, and is also used to identify and quantify known components in a mixture. Like other chromatographic methods, the components are distributed between a mobile phase (solvent, or eluent) and a stationary phase, and then separated based on the strength of interaction between the compounds in the solvent and the stationary phase in the column. In HPLC, a pump is used to provide the high pressure required for solvent to elute through the densely-packed column. This shortens the column whilst maintains the resolution compared to traditional chromatography.

For analysing amino acids, a chiral column is usually used for separation of their enantiomers. The surface of the stationary phase in the column was modified

with a crown ether, bearing the same configuration of a chiral functional group. Any molecules with a chiral centre that is positioned next to an unit of positive charge are resolved based on the affinity difference between the two enantiomers. Amino acids are the most significant application, as long as both the amino group and the carboxylate group are protonated. With the aid of a calibration curve, determination of their concentrations can also be done.

In this study, samples of histidine were analysed using a PerkinElmer Series 200 HPLC system, with a PerkinElmer Series 200 UV/Vis detector set at a wavelength of 200 nm. A 15 cm × 4 mm Crownpak CR(+) with 5 μm particles was used with a guard column, and 0.1 M perchloric acid was used as eluent at a flow rate of 0.4 mL/min. Whilst it is usual to use derivatives of the amino acids to improve separation and detection fluorescence, using the conditions outlined above allowed analysis without adding an extra derivatisation step, thereby reducing potential sources of error. Resolution of the amino acids was improved by using low pH and as low a temperature as possible. The temperature of the analysis was set at 12 °C using a Peltier plate chiller.

2.4.7 Nuclear Magnetic Resonance (NMR)

Nuclear Magnetic Resonance relies on the fact that nuclei of specific elements have angular momentum of nuclear spin. When placed in a strong magnetic field, most nuclei drop to the low-energy level (ground state) with the momentum aligning with the field, and few rise to the excited state with the momentum against the field. Nuclear magnetic resonance then occurs with applying electromagnetic radiation of a specific frequency to flip the nuclei and the relaxation then monitored.

For analysing organic compounds, ^{1}H NMR is the most commonly used technique since there is 99.985 % abundance of ^{1}H in natural hydrogen and it is highly sensitive to NMR. However, deuterated, or non-hydrogen, solvents must be used to avoid interference. To determine the identity of compounds, the chemical shift and the splitting are the key information from the NMR spectrum, where the former comes from the shielding effect from the different electron densities of different functional groups, and the latter comes from the spin-spin coupling. Other useful information is given by the peak integrals, which tells us the ratio of protons in the compound, and also, with the aid of calibration curves, can be used to determine the concentration of compounds in the solution. In this study, ^{1}H NMR was used to cross check the concentration obtained from HPLC.

With the use of sodium 3-(trimethylsilyl)-1-propanesulfonate$_{(s)}$ (TMS$_{(s)}$) as reference and D$_2$O$_{(l)}$ as solvent, ^{1}H NMR was performed on a Bruker Advance-400 spectrometer at a frequency of 400 MHz and using a pulse delay of 1 s.

2.5 Calibration and Error Assessment in Measurements

2.5.1 Production of Correlation Curves for Quantitative Analysis

High Performance Liquid Chromatography (HPLC) with a chiral column and Nuclear Magnetic Resonance (NMR) were used to determine the amount of amino acid adsorbed in the interlayer of LDH, and a correlation curve is required for both of these techniques.

A 0.1 M histidine solution was prepared with D, L-histidine$_{(s)}$ (3.8786 g, 25 mmol) in 250 mL volumetric flask. Dilutions of various concentrations were then made with an Eppendorf pipette in 5 mL volumetric flasks (see **Table 3** below for

amounts of 0.1 M histidine solution used) and transferred to marked vials.

Conc (M)	0.1 M histidine (mL)
0.06	3.00
0.04	2.00
0.02	1.00
0.01	0.50
0.005	0.25
0.002	0.01

Table 3 The amounts of D, L-histidine solution needed to prepare 5 mL D, L-histidine

across a concentration range of 0.06 M to 0.002 M.

2.5.1.1 NMR

A 0.01 M solution was prepared as an internal standard of chemical shifts using $D_2O_{(l)}$ and Sodium 3-(trimethylsilyl)-1-propanesulfonate$_{(s)}$ (TMS, 0.0439 g, 0.2 mmol) in a 20 mL volumetric flask. The solution was then transferred to a marked vial and sealed with parafilm after every use.

A 0.5 mL D, L-histidine$_{(aq)}$ of seven various concentrations were transferred to marked vials and dried in the oven at 80 °C for 24 hours. 0.5 mL of 0.01 M TMS$_{(aq)}$ and 0.5 mL $D_2O_{(l)}$ were then added to each vial, before which each was placed on shaker plate until the histidine were re-dissolved. The solutions were then submitted for ^{1}H NMR analysis.
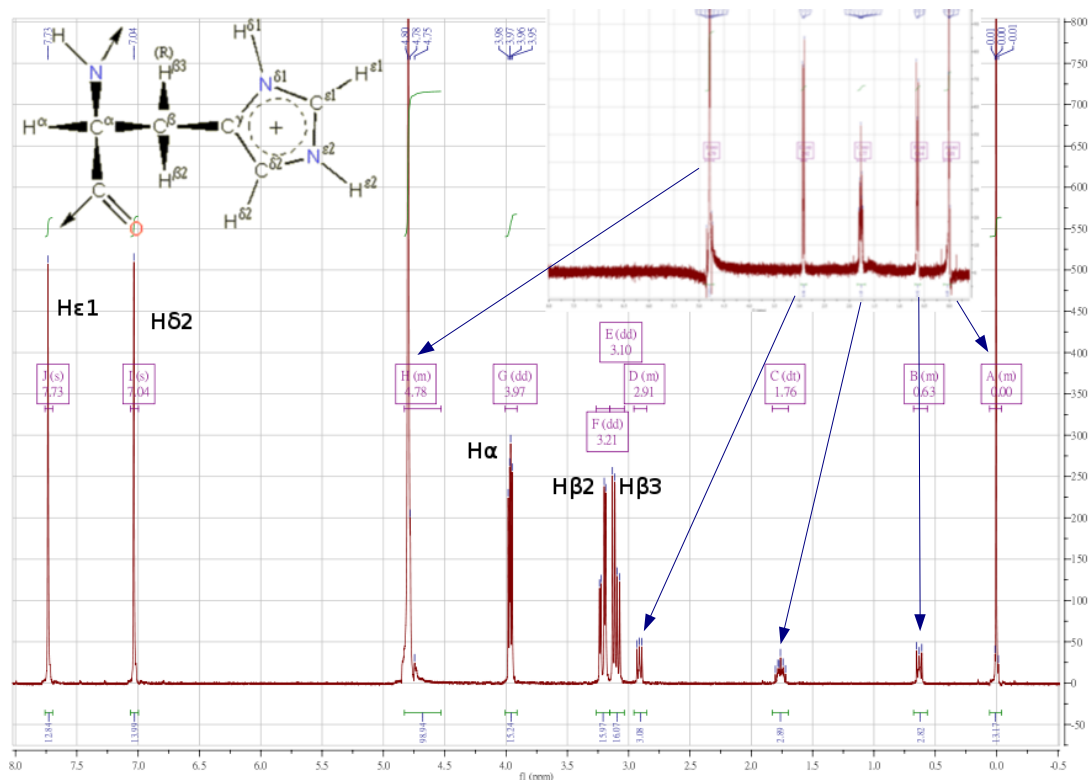
Figure 7 NMR graphs of 0.1 M D, L-histidine$_{(aq)}$ standard and water blank (small graph on the upper right) with TMS reference. From high field to low field, the peaks from the blank represent the hydrogen atoms from the three methyl on silyl, C1, C2, C3 on TMS, and water.

2.5.1.2 Chiral HPLC

A 0.1 mL D, L-histidine$_{(aq)}$ of each concentration was placed in a marked sample vial for HPLC, and 0.9 mL deionised water was added for dilution. A blank sample was also prepared with 1 mL deionised water.

Analysis process consisting of 0.1 M sample was run at various injection volumes until the maximum, non-over-ranged peaks were obtained. Samples of all other concentrations were then analysed using the same injection volume.
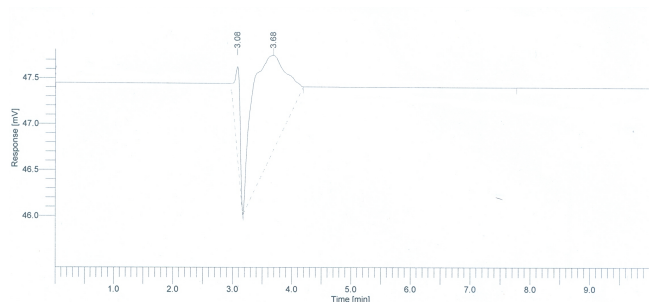
HPLC Report (HPLC 3)

Peak #	Time [min]	Area [μV·s]	Height [μV]	Area [%]	Norm. Area [%]	BL	Area/Height [s]
2	3.076	6089.40	952.19	11.77	11.77	BB	6.3951
3	3.685	45628.00	1037.72	88.23	88.23	BB	43.9694
		51717.40	1989.92	100.00	100.00		
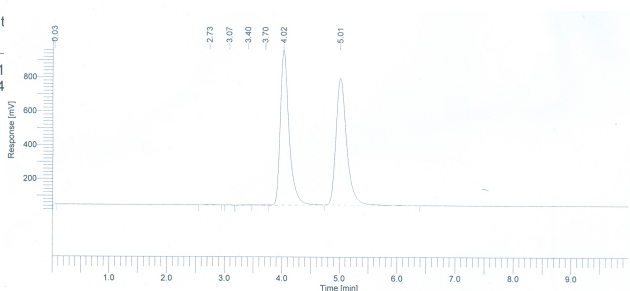
HPLC Report (HPLC 3)

Peak #	Time [min]	Area [μV·s]	Height [μV]	Area [%]	Norm. Area [%]	BL	Area/Height [s]
2	2.732	3187.20	377.50	0.02	0.02	BB	8.4429
3	3.074	5366.40	910.55	0.03	0.03	BB	5.8936
4	3.402	17955.92	1343.99	0.09	0.09	BV	13.3602
5	3.704	14798.21	688.13	0.08	0.08	VV	21.5049
6	4.021	9721570.27	918981.00	49.86	49.86	VB	10.5786
7	5.009	9734490.20	750970.74	49.93	49.93	BB	12.9625

Figure 8   The printed plots of HPLC after running water blank (left) and 0.08 M D, L-histidine$_{(aq)}$ standard (right) for calibration.

Due to the low pH conditions used for analysis, degradation of the chiral column and guard column was relatively rapid, hence correlation curves were re-produced for new columns when replaced.

2.5.2 Assessment of Random Errors

Careful measurements of calibration curves were not only used to determine the concentrations of intercalated histidine, but also to estimate the random errors

present within the analytical methods. The standard deviation for each concentration calculated from the signal of HPLC or NMR was also obtained from the standard deviation of regression line. In this case, the time used for measuring is effectively shortened, as well as the quantity of eluent of HPLC that can be saved.

	A	B	C	D
1	Concetration of standard (M)		HPLC signal (mV·S)	
2	Total	Enantiomer	4 min	5 min
3	0.08	0.04	9714.168	9716.484
4	0.06	0.03	7180.100	7165.284
5	0.04	0.02	4843.560	4827.920
6	0.02	0.01	2405.610	2392.667
7	0.01	0.005	1182.006	1169.858
8	0.004	0.002	447.330	436.104
9	0.002	0.001	221.727	212.106
10				
11	Regression line (concentration to signal)			
12		Slope	4.1213E-06	4.1180E-06
13		Intercept	1.2411E-04	1.7982E-04
14		Standard deviation	0.00015	0.00017

	A	B	C	D	E	F	G	H	I	J	K	L	M	N
1	Initial Concentration (M)		HPLC signal		Concentration after reaction (M)			Intercalated histidine (mmol)			Exchanging rate (%)			
2	Total	Enantiomer	4 min	5 min	D	L	Total	D	L	Total	D	L	Total	D-L
3	0.08	0.04	9616.945	9603.159	0.03976	0.03973	0.07948	0.04831	0.05480	0.10311	1.48%	1.68%	3.16%	-0.20%
4	0.06	0.03	7203.696	7185.733	0.02981	0.02977	0.05958	0.03745	0.04581	0.08327	1.15%	1.40%	2.55%	-0.26%
5	0.04	0.02	4809.304	4774.648	0.01994	0.01984	0.03979	0.01106	0.03160	0.04266	0.34%	0.97%	1.31%	-0.63%
6	0.02	0.01	2340.554	2305.726	0.00977	0.00967	0.01945	0.04595	0.06502	0.11097	1.41%	1.99%	3.40%	-0.58%
7	0.01	0.005	1140.443	1097.945	0.00482	0.00470	0.00953	0.03516	0.05976	0.09492	1.08%	1.83%	2.91%	-0.75%
8	0.008	0.004	902.617	839.292	0.00384	0.00364	0.00748	0.03119	0.07279	0.10398	0.96%	2.23%	3.19%	-1.28%
9	0.004	0.002	436.547	368.685	0.00192	0.00170	0.00362	0.01535	0.06039	0.07573	0.47%	1.85%	2.32%	-1.38%
10			4.1213E-06	4.1180E-06										
11			1.2411E-04	1.7982E-04										
12		Standard deviation→	0.00015	0.00017	0.00015	0.00017	0.00023	0.03068	0.03389	0.04571	0.94%	1.04%	1.40%	1.40%
13	Error bar used in graph→										1.84%	2.04%	2.75%	2.75%
14														
15												Exchangable site (mmol/g)		
16												3.2610545602		

Figure 9 The standard deviations of the analysis were obtained whilst producing the regression lines from standard solutions.

Every time a set of concentrations was run for calibration, the graphs of concentration to signal of both isomers were plot separately under LibreOffice Calc. The slopes, intercepts and standard deviations of both linear regression lines were then generated. These six numbers were used later to calculate the remaining concentration of the reacted histidine, and subsequently to the anion exchanging rates, and their standard deviations, from the signals obtained after the experiment. For both the anion exchanging rates of the D, L-histidine and the differences between enantiomers, the standard deviations were the same value, the square root of the

29

square sum of individual standard deviation. Finally, the 95 % confidence intervals, if needed, were obtained from the standard deviations multiplied with the factor 1.96 (see Appendix).

2.5.3 Systematic Error from HPLC

In the total 10-minute time of elution, the peaks for D- and L- forms of histidine appeared at about 4 minutes and 5 minutes, respectively. There were also peaks from the blank around 3 minutes, a positive one followed by a negative one. When the concentration of histidine was less than 0.01 M, the programme would automatically redraw the baseline from the negative peak all the way to the end of peak of L-histidine. This increased the areas of both D- and L-histidine but more of the D-histidine, changing the ratio between two forms and deviating the linear correlation between concentration and HPLC signal.
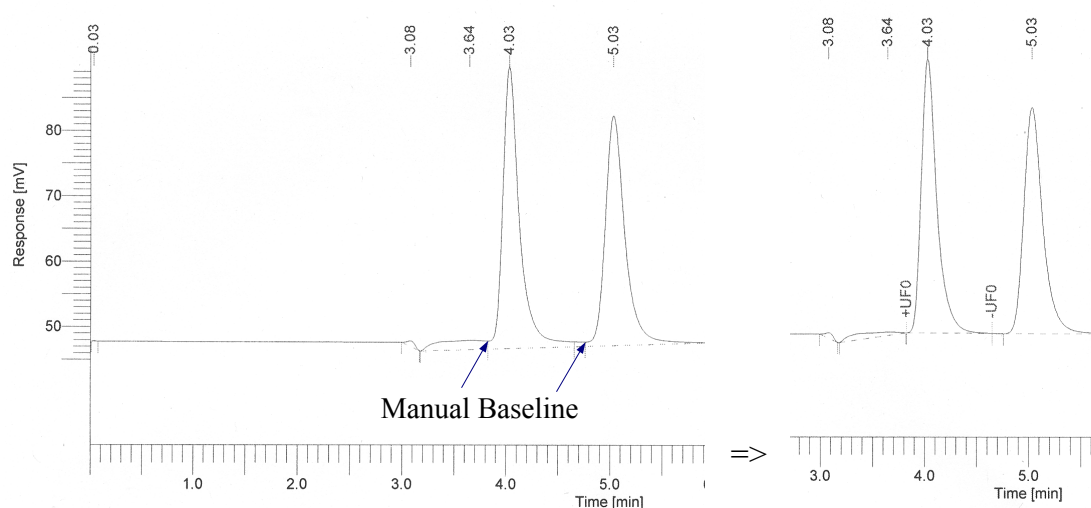
Figure 10   The dash line in the left is the programme-drawn baseline. By using "Manual Baseline" to connect the starting points of two peaks on the original baseline, the bias is reduced.

30

To correct this deviation, every time the bias baseline appeared the "Manual Baseline" in programme needed to be re-done. By manually redrawing the baseline of D-histidine, the programme would also auto-modify the part of L-form. This effectively restored the linear relationship between the HPLC signal and the histidine concentration, and therefore reduced the bias in measurement.

3. Synthesis and Characterisation of Chloride Intercalated Layered Double Hydroxides (LDH-Cl)

There are several techniques that have been successfully employed in the preparation of LDHs, as described below. The most commonly used are those based on co-precipitation methods.[49, 63] Co-precipitation has the advantage of allowing a one-pot direct synthesis of LDHs containing a variety of metal cations and interlayer anions, even for those of organic anion-containing ones which are sometimes difficult to synthesise by other process.[64] Unlike certain other methods of synthesis, co-precipitation allows the possibility of large-scale synthesis and, as such, tends to be the first choice method for LDH preparation. A second method is based on the ion-exchange process, in which the guests are exchanged with the anion present in the interlayer of host LDH.[35] The ion-exchange method is especially useful when the desired anion to be intercalated in the LDH is unstable in alkaline solution, or the direct reaction between the metal ions and anion of choice is more favourable, making the one-pot co-precipitation inapplicable. Another method, the reconstruction reaction, is based on the so-called "memory effect" of layered double hydroxides.[65] In this method, calcination of LDHs removes the interlayer water, interlayer anions and the hydroxide groups, resulting in a mixed metal oxide that can be reconstructed to LDHs by exposing to water and the target anions. Other methods, such as the sol-gel synthesis,[66] and a fast nucleation process followed by a separate aging step at elevated temperatures,[67] have also been used for LDH synthesis.

Two methods of co-precipitation have been commonly used: precipitation at low supersaturation and precipitation at high supersaturation. The former is performed by adding a mixed solution of divalent and trivalent metal salts in the

desired ratio into a reactor containing an aqueous solution of the target interlayer anion, whilst an alkaline solution is added simultaneously to control the pH in the reactor at a selected value. On the other hand, the latter is prepared by addition of a mixture of metal salts solution into the alkaline solution containing the desired interlayer anion. Due to the high number of crystallisation nuclei, synthesis at high supersaturation is more likely to obtain less crystalline materials.[65]

An important step after precipitation is aging. Once the metal solution is all added, the mother liquor, heated at the reaction temperature under an inert gas atmosphere, is stirred for between a few hours and several days. Compared to the raw, un-aged LDH, the aging process tends to lead to better cation order and crystallinity. This can be differentiated through the PXRD analysis results, whilst the aged LDH shows sharper and more intense diffraction peaks. The mechanism of this process is called Ostwald ripening.[65] Since the molecules, or ions, on the surface are energetically unstable compared to the ones in the interior, it is thermodynamically favoured to form particles with larger portion of internal molecules or ions, i.e. particles with larger size. Therefore, during the process of aging, small crystals tend to dissolve and re-precipitate into larger ones, and a more uniform size distribution of LDH crystals will be obtained at the end of the aging process.

After aging, the precipitate was then separated from its mother liquor, and washed with deionised water two or three times to remove any unreacted cations and anions.

3.1 Physical Properties

It has been observed that, despite efforts to maintain consistent preparation technique, considerable variation may be encountered between compositionally

identical LDH preparations. By way of example, once after drying in the oven, variation was shown in the physical/mechanical properties between various preparations of LDHs. When being ground with a mortar and a pestle, samples of DL_LDH0110 and 0120 were found to be mechanically harder than the other samples, making it take longer to grind the sample into a fine powder. Differences were also shown in their densities. These density differences were distinguishable after the samples were weighed into the sample vials. For the samples that were harder to grind, less than 1/2 the height of other samples was loaded in the sample vials even though there was approximately the same weight for every sample (DL_LDH 0110 and 0120, **Figure 11**). This may come from the size differences of crystal, with the harder and denser one being larger in crystal size, which may be caused by dropping and stirring speeds differences during co-precipitation.
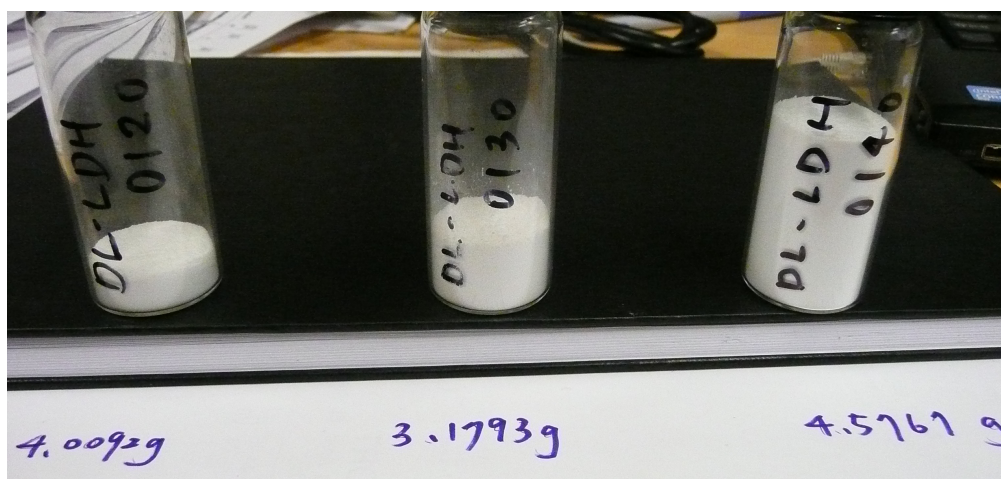
Figure 11 Photograph to show the density changes for apparently very similar sample preparations. The the ratio of approximated volumes and the weights of three different preparation of LDH-Cl are clearly visible.

3.2 Determination of Empirical Formula

From elemental analysis, it is found that the LDHs contain about 0.30 % ~ 0.66 % of element carbon, which suggested that small amounts of carbonate ions ($CO_3^{2-}{}_{(aq)}$) had been incorporated in the interlayer space of the LDHs. This is not surprising since carbon dioxide ($CO_{2(g)}$) is highly soluble in high-pH solutions where it reacts to form carbonate. Even though nitrogen ($N_{2(g)}$) flow was used during the synthesis steps and 24-hour aging of the co-precipitation reaction, contamination during preparation of the $NaOH_{(aq)}$ used to attain pH 10 is almost impossible to avoid. There was also 3.45 % ~ 3.78 % of element hydrogen in the samples. Whilst about 0.80 % ~ 1.20 % of those come from interlayer water, others came from the hydroxyl groups in the metal layers. Finally, the content of nitrogen in every sample was zero, as expected.

From the ICP-OES data, the magnesium content in the LDHs are between 17.2 % and 19.9 %, and those of aluminium are between 10.0 % and 10.8 %. The ratios of Mg/Al are between 1.82 and 2.05. The lower ratio of Mg/Al, i.e. more aluminium in the layers, means there is a higher charge density present in layers. Combining the data of these two analyses, the empirical formula of the synthetic LDHs can be calculated.

The theoretically ideal formula of Mg_2Al-Cl LDH is $Mg_2Al(OH)_6Cl \cdot zH_2O$ (rather than the general formula of LDHs, $[M^{2+}{}_{1-x}M^{3+}{}_x(OH)_2]^{x+}[A^{n-}]_{x/n} \cdot yH_2O$, that has been used in most literature; this one is used here to aid understanding and calculations). The ideal formula can be converted into a practical one that can be used with the assumptions below:

1. The structure in layers is still perfect, with only the substitution of aluminium

ions by magnesium ions not making the molar ratio of Al/Mg perfect 1/2, i.e. the formula in layers is $Mg_{(2+x)}Al_{(1-x)}(OH)_6$.

2. There were some chloride ions substituted by carbonate ions in the interlayer, with the total negative charge equal to the positive charge in layers, i.e. the formula of anions in interlayers is $Cl_{(1-x-2y)}(CO_3)_y$.

As a result, the assumed formula used for calculating is:

$$Mg_{(2+x)}Al_{(1-x)}(OH)_6Cl_{(1-x-2y)}(CO_3)_y \cdot zH_2O \qquad \textbf{Formula 2}$$

	%C	%H	%Al	%Mg	Formula	g/mol	(mmol ex)/g
0100	0.32	3.45	10.74	19.87	$Mg_{2.02}Al_{0.98}(OH)_6Cl_{0.86}(CO_3)_{0.06} \cdot 0.9H_2O$	228.03	3.7760
0110	0.42	3.78	10.51	19.39	$Mg_{2.02}Al_{0.98}(OH)_6Cl_{0.82}(CO_3)_{0.08} \cdot 1.46H_2O$	237.92	3.4381
0120	0.38	3.64	10.00	17.21	$Mg_{1.97}Al_{1.03}(OH)_6Cl_{0.88}(CO_3)_{0.07} \cdot 1.27H_2O$	236.27	3.7305
0130	0.66	3.76	10.71	17.61	$Mg_{1.94}Al_{1.06}(OH)_6Cl_{0.8}(CO_3)_{0.13} \cdot 1.49H_2O$	240.93	3.3089
0140	0.66	3.67	10.75	18.52	$Mg_{1.97}Al_{1.03}(OH)_6Cl_{0.77}(CO_3)_{0.13} \cdot 1.3H_2O$	236.28	3.2611

Table 4 Composition of selected prepared layered double hydroxide minerals based on analytical data.

3.3 Determination of Structure

From the results of TGA/MS, the stages of decomposition under heating could be determined, and, therefore, details of the structure could be obtained. The following data was obtained from the mass spectrometer for H_2O, HCl, and CO_2:

1. Water: Two groups of ions with m/z 18 were obtained. In the first, heating up

to 150 °C, the interlayer water was lost. Quick release of water from the interlayer was predictable since it, as the only charge neutral particle in LDHs, has the weaker hydrogen bond rather than stronger ionic or covalent bond to other particles.[36] At 200 °C – 500 °C, dehydroxylation of the LDH hydroxide layer gave rise to the second water peaks From the sample of DL_LDH 0100 and 0130, there was splitting in the latter peaks, which means the hydroxyl groups in layers were not in the same environment. This may explain why these two samples are softer and larger in volume than others since their structures are not perfect to form homogeneous, compact crystals.

2. Hydrogen chloride: HCl was released in almost the same temperature interval as dehydroxylation since each chloride in the interlayer needs to gain a hydrogen atom from hydroxyl groups in the metal hydroxide layers to form hydrogen chloride before being released. Additionally, structural changes must occur to ensure the residual structure remains charge balanced.

3. Carbon dioxide: With only minor carbonates in the interlayers, release of CO_2 did not cause as much weight decrease as loss of water and hydrogen chloride. The peaks due to carbon dioxide were shown earlier in the heating cycle, before those of hydrogen chloride and second water, but later than the peaks of the interlayer water. This was owing to the energy needed for decomposing carbonate into carbon dioxide being smaller than decomposition of the hydroxide groups in the layers, but still larger than release of water from the interlayers.

Powder XRD was the other technique used here to determine the detailed structure of the LDH materials. Since Mg_2Al-Cl LDH is usually described as 3**R** polytype with $R\bar{3}m$ (rhombohedral) symmetry,[61] reflections are systematically absent unless their hexagonal Miller indices h, k, l are in the rule of $-h + k + l = 3n$. By this rule, the common reflections of LDH-Cl are 003, 006, 012, 015, 018, 110, and 113.
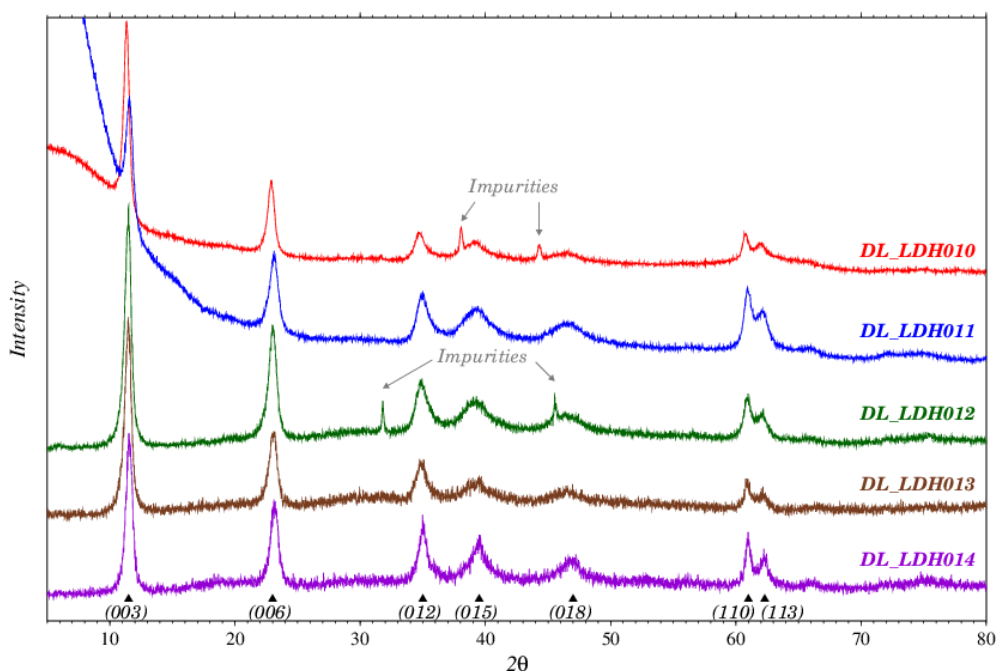
Figure 12   Powder XRD patterns of the prepared layered double hydroxide chloride materials.

The first piece of information that can be obtained from the XRD pattern was c_0, which equals the thickness of one brucite-like layer plus one interlayer. It could be directly calculated from the lowest angle reflection, 003, and the unit cell parameter $c = 3c_0$ for 3**R** polytype LDHs. The other way, which is more precise, is to obtain c_0 is by calculating the d-spacing from both the 00l reflections:

$$c_0 = \frac{d_{003} + 2\,d_{006}}{2} \qquad \textbf{Equation 3}$$

The second piece of structural information was the lattice parameter a_0 calculated from the high angle reflection 110, where $a_0 = 2d_{110}$. This value corresponds to the distance between two adjacent metal cations. Therefore, it is dependent on the ratio of divalent and trivalent metal ions, for the more trivalent ions in the hydroxide layer, the smaller the hydroxide-metal bonds, and the closer the cations are situated in the layer. The cation ratio also affects the c_0 parameter, since the larger charge density in layers shortens the distance between layer and interlayer.

	d_{003}	d_{006}	c_0	d_{110}	a_0
DL_LDH0100	7.8014	3.8831	7.7838	1.5243	3.0485
DL_LDH0110	7.6481	3.8319	7.6560	1.5210	3.0419
DL_LDH0120	7.6947	3.8602	7.7076	1.5198	3.0397
DL_LDH0130	7.7215	3.8437	7.7045	1.5212	3.0424
DL_LDH0140	7.6549	3.8405	7.6679	1.5194	3.0388

Table 5 The a_0 and c_0 parameters of the prepared layered double hydroxide materials in angstroms.

The last part from the XRD graph is the reflections of 01l at intermediate angles, which allow us to determine the stacking pattern of the layers.

In the adsorption experiments, the DL-LDH 011, 013 and 014 were used whilst the DL-LDH010 and 012 were left. This is because there are unknown reflections, which were speculated to be due to impurities, MgO in 010 and NaCl in 012, having a possible influence to the results of adsorption experiments.

4. Effect of pH on Anion Exchange of Histidine by Chloride-Layered Double Hydroxide Minerals

Histidine, with an imidazole group in its side chain, was used in this study to mimic the adsorption reactions of a basic amino acid on the prebiotic Earth. Owing to the aromatic ring which absorbs electromagnetic radiation that falls in the range of UV/Vis (200 nm – 400 nm), the concentration of histidine could be effectively determined by High Performance Liquid Chromatography (HPLC) with an integrated UV/Vis detector. The intercalation properties of histidine have also been studied into Mg_2Al-Cl LDH and vermiculite, by Ikeda *et al.*[56] and Fraser *et al.*[84] respectively, allowing the comparison with the experiments presented here.

(A)

(B)

his^-	his^{+-}	his^{++-}	his^{++}
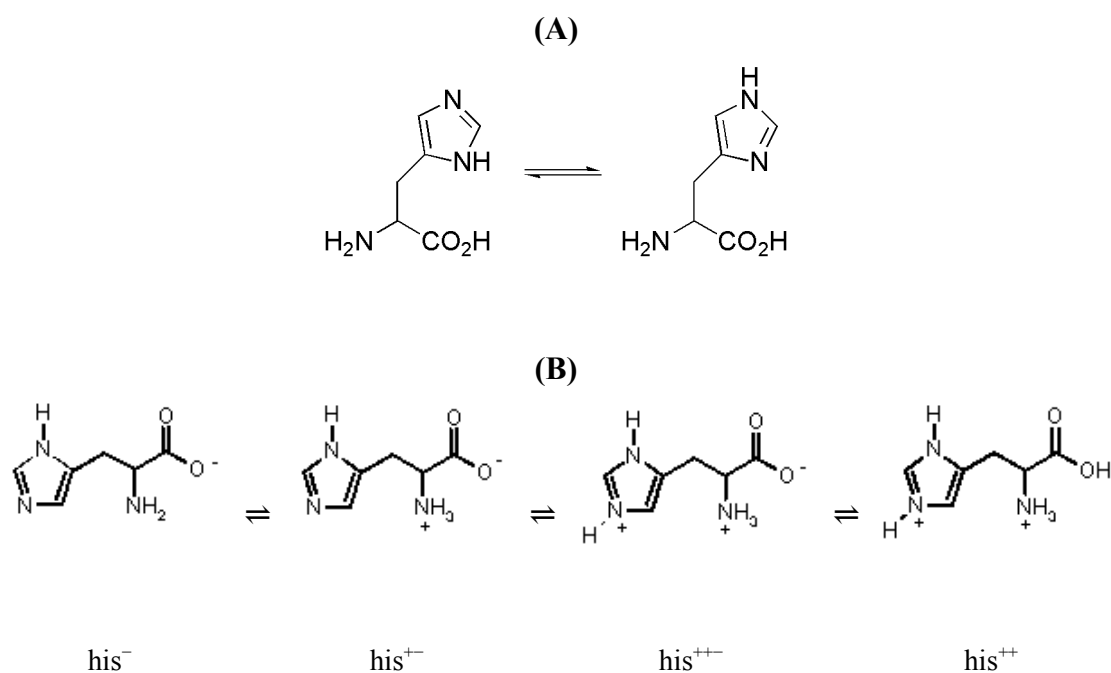
Figure 13 **(A)** The resonance structure of imidazole group in histidine and **(B)** the ion forms of histidine with different charges.

There are three pK_a for histidine: 1.82 for the carboxylic acid, 6.02 for imidazole ring, and 9.17 for the amino group. This means that it bears an average charge, ranging from +2 to −1, depending on the pH value across a wide range. This property was utilised in both analytical and experimental aspects of this study.

For quantitative analysis of the amount depleted from solution, a chiral column in HPLC (introduced in Section 2.4.6) was used to separate the D- and L-forms of histidine. Considering the maintenance of the stationary phase in the column and the pK_a of histidine, 0.1 M perchloric acid, a solution at pH 1, was used as eluent, as well as a proton source, in HPLC analysis carried out in this work.

The pH value is also related to the net charge of histidine in adsorption experiments. Since only anions intercalate into the LDH interlayers, the amount of histidine adsorbed by the LDHs was certainly related to the percentage of histidine bearing net negative charge, which could be calculated by the Henderson-Hasselbalch equation.

4.1   Results and Discussion

4.1.1 Anion Exchange at pH 7

At pH 7, 0.61 % of histidine bears one net negative charge (none of its groups, amino, carboxylate and imidazole, is protonated), being the form that can exchange with chloride, whilst about 90 % is zwitterion. The rest, i.e. 9.42 %, bears a unit positive charge, as a result of positive charges on both amino and imidazole groups and a negative charge on carboxylate.
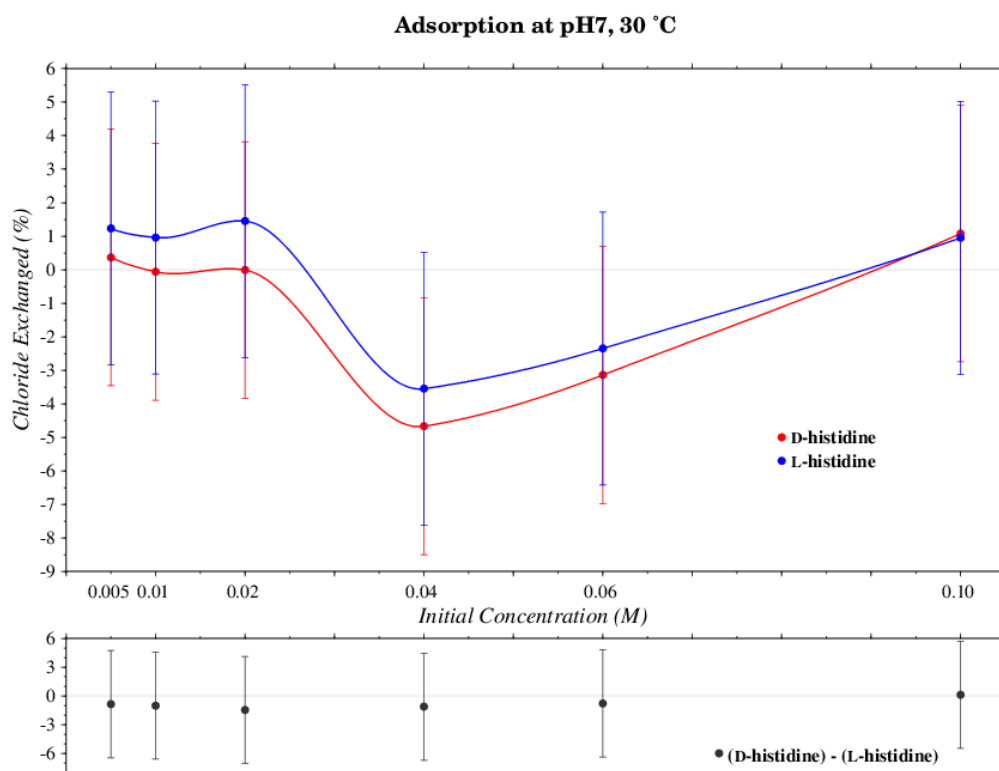
Figure 14   The percentage of interlayer chloride exchanged by D- and L-histidine in the reaction at pH 7, 30 °C, and the differences between enantiomers (lower part). The error bar is the 95 % confidence interval (see Appendix for numbers) of each estimate.

However, the results from HPLC showed unexpected adsorption isotherms (see **Figure 14**). There were negative exchange rates in both D- and L-histidine in the solutions of 0.06 M and 0.04 M, and also D- form in 0.02 M and 0.01 M solutions. It means that in these solutions the histidine particles were more concentrated after the adsorption reaction.

Moreover, in retrospect, it was discovered that an error was made when preparing the histidine solution at pH 7. With the overall $pK_a = 6.5$, histidine can be treated as a weak acid in solution: base or buffer should have been added to adjust the pH to 7. Therefore, the actual pH of histidine at pH 7 reaction needed to be

calculated, as well as the portion of each form in every concentration used (see **Table 6** below).

Conc (M)	pH	his^-/his^{+-}	his^{+-}/his^{++-}	his^{++-}/his^{++}	his^-(%)	his^{+-}(%)	his^{++-}(%)	his^{++}(%)
0.1	3.75	3.80×10^{-6}	5.37×10^{-3}	85	0.00	0.53	98.32	1.16
0.06	3.86	4.41×10^{-6}	6.93×10^{-3}	110	0.00	0.68	98.42	0.90
0.04	3.95	6.01×10^{-6}	8.49×10^{-3}	135	0.00	0.84	98.43	0.73
0.02	4.10	8.50×10^{-6}	1.20×10^{-2}	190	0.00	1.18	98.30	0.52
0.01	4.25	1.20×10^{-5}	1.70×10^{-2}	269	0.00	1.66	97.97	0.36
0.005	4.40	1.70×10^{-5}	2.40×10^{-2}	381	0.00	2.34	97.40	0.26
Any	7	6.76×10^{-3}	9.55	1.51×10^5	0.61	89.97	9.42	0.26
	pK_a	9.17	6.02	1.82				

Table 6 Calculated pH values of 6 solutions and the portions of histidine ions in pH 7 reaction. The last one is the expected portions if the reaction was run at pH 7.

Table 6 describes the condition of each histidine solution before 250 mg of LDH powder was added. However, LDHs are unstable when the pH is below 5, and the dissolution becomes even faster when the pH drops below 4.[68] Therefore, once the LDH was added, dissolution occurred through the reverse reaction of the equilibrium below:[69]

$$Al(OH)_{3(s)} + 2Mg^{2+}_{(aq)} + 3OH^-_{(aq)} + Cl^-_{(aq)} \rightleftharpoons Mg_2Al(OH)_6Cl \quad \textbf{Equilibrium 1}$$
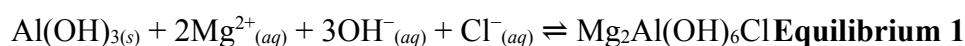
With the solubility product $K_{sp} = 3\times10^{-34}$,[70] there is only trace $Al^{3+}_{(aq)}$ dissolved from $Al(OH)_{3(s)}$ ($[Al^{3+}_{(aq)}] = 3\times10^{-4}$ M at pH 4) even though the concentration of hydroxide anion ($OH^-_{(aq)}$) is extremely low. Also, histidine ions can play the role of buffer, releasing hydrogen ions to recover those being neutralised by hydroxide from dissolution of LDH. All these factors made the reaction very unpredictable.

Due to the rapid dissolution of LDHs at pH values below 4, there should be no histidine exchanged by interlayer chloride in the 0.1, 0.06, and 0.04 M solutions. From the negative exchanging rates in 0.06 and 0.04 M, it was speculated that the solutions were more concentrated after the reaction. One possible explanation for this would be loss of water from evaporation. During the 24-hour reaction, nitrogen flow was used to reduce the potential of competitive intercalation of carbonate ions from solution capture of carbon dioxide in the air. Since the partial pressure of vapour water was zero from the nitrogen cylinder, the reacting solutions were the first sources of water vapour, supplying water molecules to the circulating nitrogen flow, which exited the reactor later. The phenomenon of liquid loss was not obvious to a level to be discovered until the first reaction at 60 °C was run. The procedure was then modified for the upcoming experiments to eliminate this systematic error, but the reactions at 30 °C at pH 7 (and also at pH 10) were not re-run.

Dissolution of LDH was slower at pH above 4, making the intercalation of histidine still possible in the 0.02, 0.01 and 0.005 M solutions. However, the best form of histidine to intercalate, histidine anion, barely exists at this pH. The other way for histidine intercalation is the zwitterion co-intercalated with an anion. As reported by Aisawa et al.,[71] phenylalanine and glycine, in their zwitterion forms, are able to intercalate into Zn-Al LDH with aid of co-intercalating nitrate anion (NO_3^-). Since the loss of hydroxides in layers by neutralisation is the cause of dissolution, anions that can be used are those which may be dissolved from the prepared LDH-Cl interlayer, i.e. chlorides and carbonates. It is speculated that the histidine zwitterions are bonded with these anions through electrostatic force, forming coupled anions that can exchange with chlorides in the undissolved LDH-Cl.

4.1.2 Anion Exchange at pH 10

At pH 10, the portions of histidine ions were different from those at pH 7. Most of the histidine in solution appeared as an anion, bearing only one negative charge on the carboxylate group, with this being the format that is most readily intercalated into LDHs. Portions of each form are shown in the table below.

Conc (M)	pH	his^-/his^{+-}	his^{+-}/his^{++-}	his^{++-}/his^{++}	$his^-(\%)$	$his^{+-}(\%)$	$his^{++-}(\%)$	$his^{++}(\%)$
Any	10	6.76	9.55×10^3	1.51×10^8	87.11	12.89	0.00	0.00
	pK_a	9.17	6.02	1.82				

Table 7 Portions of histidine ions at pH 10.

Under the condition of pH 10, the largest amount of adsorption was using 0.06 M histidine, with 0.103 mmol of histidine adsorbed by LDH-Cl, and exchanging 12 % of interlayer chloride. This exchanging rate stays at about 8 % in 0.04 M and 0.02 M of histidine, and drops to 3 % from 0.01 M to 0.004 M. In the solutions below 0.04 M, the adsorption isotherm followed the Langmuir model,[72] having a rapid initial uptake, followed by maximum uptake from solutions.

In a previous study by Hibino in 2004,[49] enantio-pure L-histidine anion was able to intercalate into Mg_3Al-LDH by co-precipitation methods at pH 10, where the LDH was prepared directly in the presence of the amino acid, with histidine occupying up to 26.5 % of interlayer anion sites created by aluminium ions. The charge occupation by amino acid was higher than attained here, possibly because the intercalation in co-precipitation proceeded in the presence of excess histidine anions, which could be co-precipitated into LDH directly.
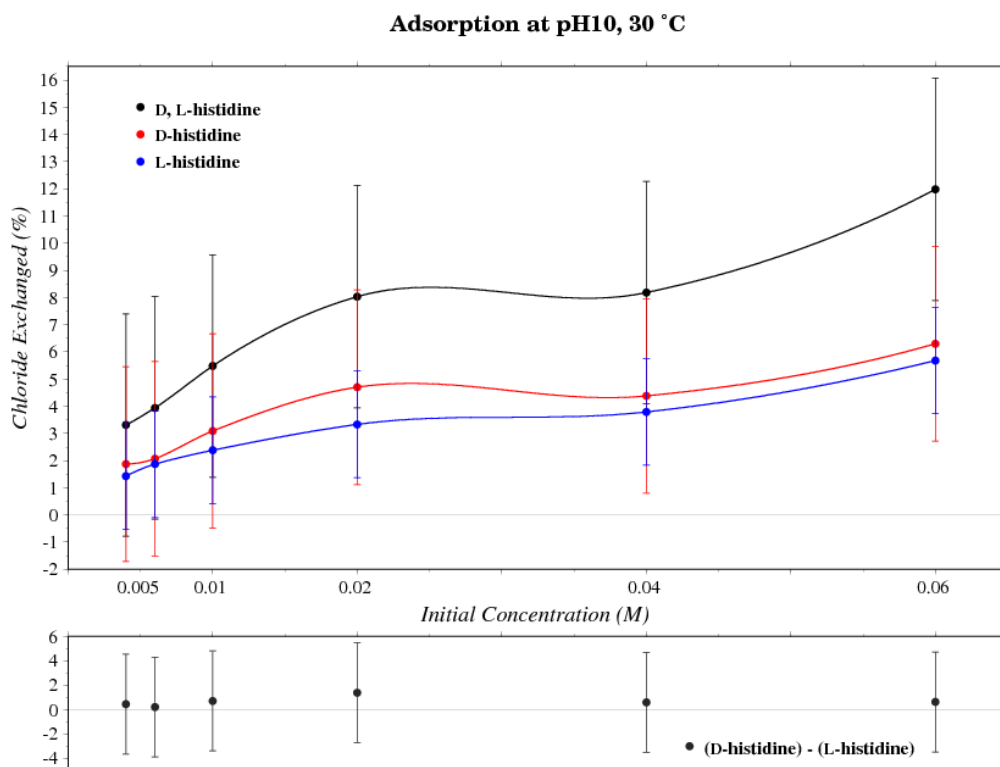
Figure 15 The percentage of interlayer chloride exchanged by D- and L-histidine at pH 10, 30 °C, and the differences between enantiomers (lower part). The error bar is the 95 % confidence interval (see Appendix for numbers) of each estimate.

For individual enantiomers, the LDH-Cl took up greater amounts of D-histidine than L-histidine. The largest difference between the D- and L-histidine was in 0.02 M solution and the smallest in the 0.006 M solution, but none were significantly different in all concentrations, based on the intervals of a 95 % confidence level. This means that there was no obvious difference between the amounts of intercalated D- and L-histidine, and therefore, it was speculated that there was no significant chiral selection in the intercalation of D, L-histidine into Mg_2Al-Cl LDH in the experiment at pH 10, 30 °C.

46

5. Effect of Temperature on the Adsorption of Histidine by Layered Hydroxide Minerals

Temperature is an important factor in various aspects of LDH chemistry, including having effects on: structure, stability, and intercalation behaviour. Structurally, the stacking sequence of synthetic LDHs changes as a function of temperature, as reported by Hines and Solin.[73] These authors reported that the XRD pattern of a Zn/Al-Cl LDH showed that it existed as the $3\mathbf{R}_1$ polytype at ambient temperature, but transformed to the $2\mathbf{H}_1$ polytype when heating up to 150 °C with partial dehydration. Similar research has also been done by Vaysse *et. al.*, showing that a Ni^{II} /Co^{III}-CO_3 LDH with $3\mathbf{R}_1$ structure was converted to an $1\mathbf{H}$ polytype with a reduced spacing on heating at 200 °C.[74]

The temperature used in synthesis was also related to the stability of organo-LDHs. Work undertaken by Ogawa and Asai indicated that hydrothermal treatment at 150 °C during the post-co-precipitation aging process changed the stability of Mg_2Al-terephthalate LDH.[75] The interlayer terephthalate (TA) maintains the vertical (perpendicular to the inorganic sheets) orientation up to 250 °C for the non-hydrothermally treated sample, whereas the interlayer region of the hydrothermally treated one collapsed to form the structure with horizontal (parallel to the inorganic sheets) TA at 200 °C, starting from a mix of both vertical and horizontal TA at intermediate temperature of 75 °C.[76]

The effect of temperature on adsorption kinetics and selectivity by LDHs was studied by Lostch *et al.*, 2001.[77] The $LiAl_2$-LDH ($[LiAl_2(OH)_6]Cl \cdot zH_2O$, same total charge number in hydroxide layer as $Mg_2Al(OH)_6Cl \cdot zH_2O$, with Al substituted with Li and Mg substituted with Al) was used for intercalation of nucleoside

monophosphates with three different nucleobases: adenine, gaunine, and cytosine. The competition between adenosine-5'-monophosphate (AMP) and gaunosine-5'-monophosphate (GMP) resulted in different selectivity in a series of exchange reactions at different temperatures: 64.5 (AMP):35.5 (GMP) at 40 °C, 28.6:71.4 at 60 °C, and 13.5:86.5 at 80 °C. Whilst the inverse of the observed AMP/GMP ratios, the other two pairs, cytidine-5'-monophosphate (CMP)/AMP and CMP/GMP, stayed in the same trend in selectivity in this range of temperature, with CMP:AMP ≈ 80:20 and CMP:GMP ≈ 74:26.

5.1   *Results and Discussion*

5.1.1 Adsorption isotherm

The results of adsorption experiments at 60 °C (see **Figure 16**) showed the same trend of adsorption isotherm as those at 30 °C. The largest amount of histidine uptake was in the 0.06 M solution, with 0.055 mmol of histidine intercalating into the LDH-Cl and exchanging 6.7 % of interlayer chloride ions. The chloride exchange stayed at the level of about 3.9 % in 0.04 M and 0.02 M histidine, and fell to 0.75 % from 0.01 M to 0.004 M of histidine. Basically, the adsorption isotherm followed the Langmuir model,[72] having a maximum uptake from solutions, when the concentrations was lower than 0.04 M.

Although there was a similar trend in terms of histidine uptake as a function of concentration, the total amount adsorbed at 60 °C were lower than those at 30 °C. One possible contribution to this phenomenon was from the instability of the host lattice layer. With increased temperature, the larger scale of thermal undulations and/or lattice disruption may reduce the intercalation of histidine.[78]

Adsorption at pH10, 30 ˚C v.s. 60 ˚C
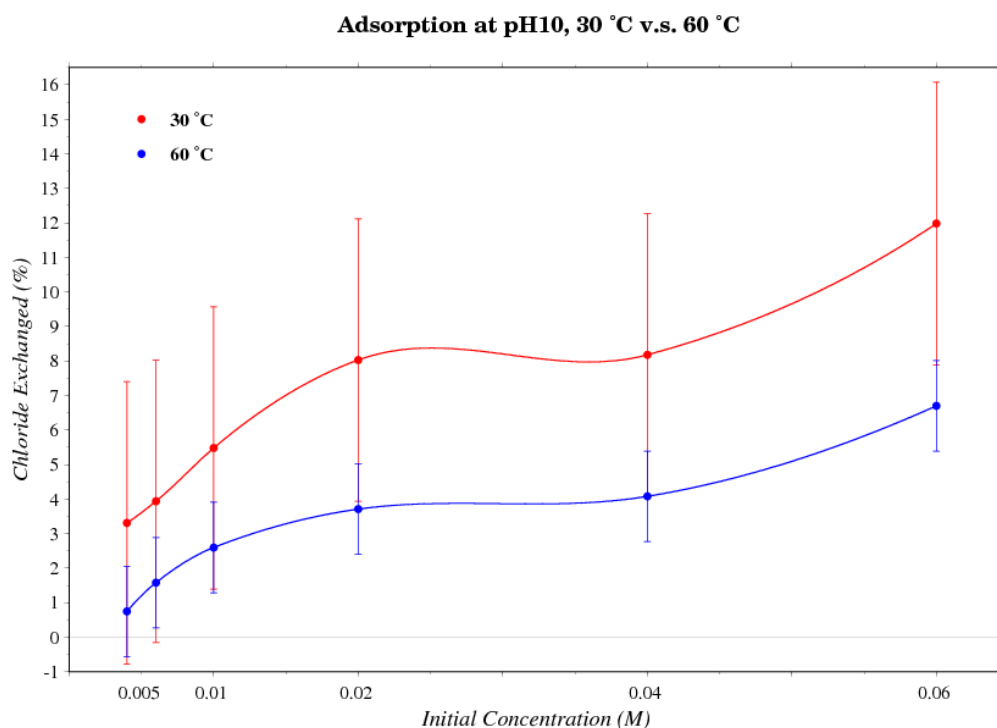
Figure 16   Comparison between the adsorptions of D, L-histidine at 30 °C and 60 °C at pH 10. There is a similar pattern in both conditions, but for each concentration at 60 °C, fewer histidine anions were intercalated into LDH.

Another possible explanation was the change of mechanism of intercalation. It is known that the ion-exchange of LDHs in aqueous solution is usually considered as a multi-step process, starting from second-order, sometimes even higher order then second-order, staging to the first-order staging before going to completion (see **Figure 17** below). However, Williams *et al.*.[79] mentioned that a transition temperature of 60 °C exists for phosphonate ions intercalated into $LiAl_2$-Cl LDH, above which the reaction proceeded only in stage-1 phases. Thyveetil *et al.*[80] undertook further research in the intercalation of DNA strands, duplex dodecamer, through computer simulation, and found that within the interlayer plane, the diffusion coefficient of the

stage-2 phase was larger than that of the stage-1 system. Similarly, as reported by Williams *et al.*,[81] the intercalation of 2-(2-methyl-4-chlorophenoxy)-propionic acid (mecoprop) into LiAl$_2$-Cl LDH underwent a change from a nucleation controlled mechanism to a diffusion controlled one as an effect of temperature.
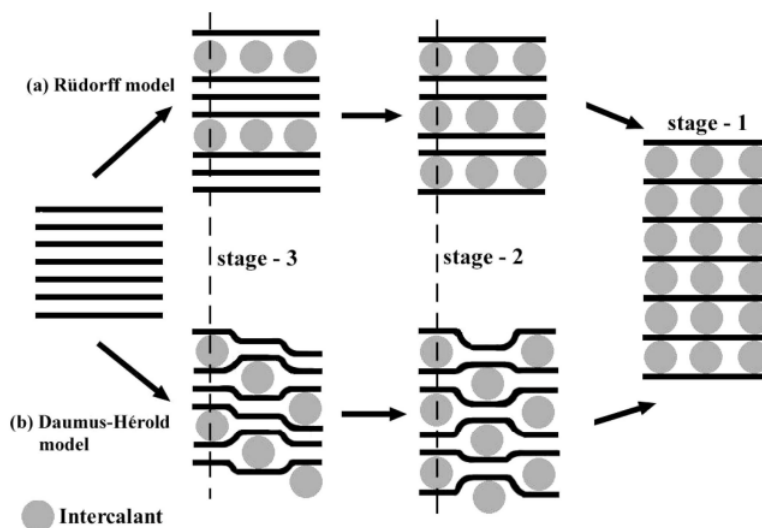
Figure 17   Staging structures during intercalation. Stage-1 compounds have guest intercalants in every interlayer; stage-2 compounds have guest intercalants in every other interlayer; stage-3 compounds have intercalants occupying every third interlayer space (taken from Thyveetil *et al.*, 2008).[80]

In view of the prior work outlined above, it was speculated that there was also a transition of staging mechanisms between 30 °C and 60 °C for the intercalation of histidine, and therefore the lower diffusivity at 60 °C reduced the amounts of exchange of histidine with chloride in the LDH interlayer.

5.1.2 Chiral selectivity

For chiral competition in the histidine adsorption at 60 °C, the trend seemed to

reverse compared to the results observed at 30 °C. In most of the concentrations tested, the LDH-Cl exchanges more L-histidine, with larger differences in 0.06 M and 0.04 M and smaller in 0.02 M, 0.01 M and 0.006 M. The only exception was in the 0.004 M, which had more of the D-His form adsorbed by the LDH-Cl.
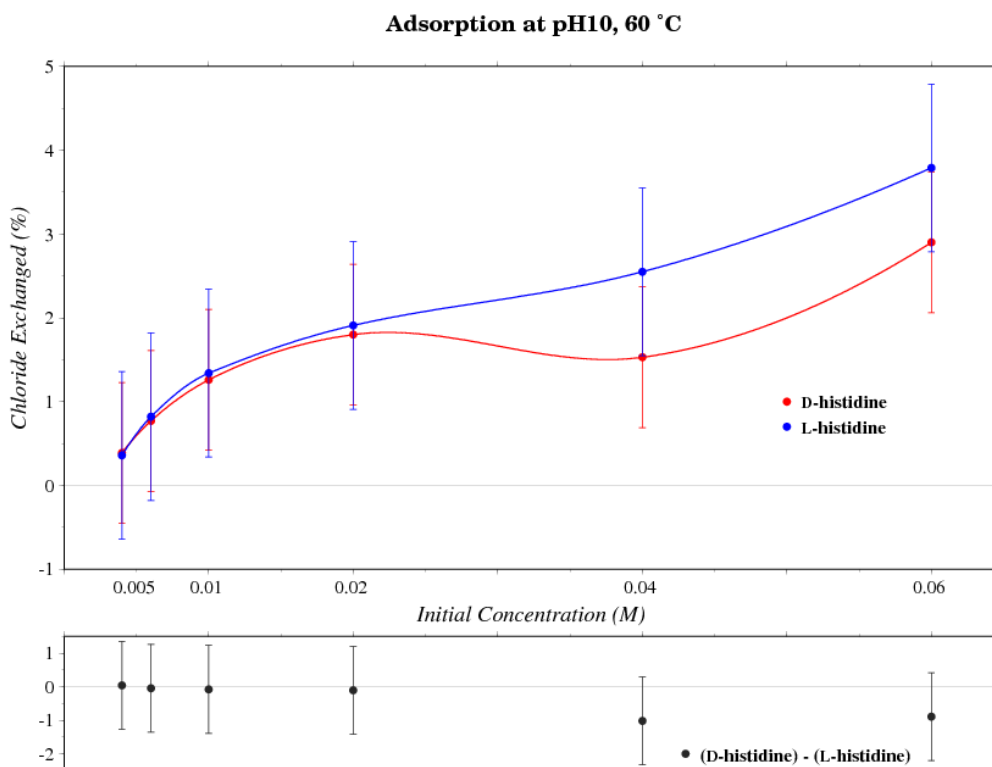
Figure 18 The percentage of interlayer chloride exchanged by D- and L-histidine at pH 10, 60 °C, and the differences between enantiomers (lower part). The error bar is the 95 % confidence interval (see Appendix for numbers) of each estimate.

However, even the largest difference between two enantiomers was not able to overcome the standard deviation from HPLC analysis, telling us that there is a significant difference with 95 % confidence level. In this case, it was speculated that there was no significant chiral selection in the intercalation of D, L-histidine into Mg$_2$Al-Cl LDH in the experiment at pH 10, 60 °C.

5.2 Geochemical Context of the Origin of Life

If the hypothesis of the origin of life occurring in alkaline hydrothermal vents is considered, it is postulated that the seepage of crust exhales material-rich hydrothermal fluids at about 100 °C and pH 10 to the seawater at 2 °C and pH 6,[7, 82] resulting in gradients of temperature and pH level around the seepage. Reactions potentially leading to the origin of life thus are able to proceed, based on catalysis by minerals.

Comparing the results of adsorption isotherms at 30 °C and 60 °C, more histidine was intercalated into the LDH-Cl at 30 °C; in terms of chiral selection, there was no significant evidence of enantio-selectivity in intercalation of D, L-histidine at both 30 °C and 60 °C. Since the amount of intercalated histidine was the only consideration available here, it was then speculated that the reaction at 30 °C fitted better to the hypothesis of life having started in hydrothermal vents.

Owing to the temperature gradient of hydrothermal fluids being from about 100 °C to 2 °C, it is worth investigating if other temperatures in this region could be even better conditions for histidine intercalation and chiral selection, for example, 80 °C and 50 °C.

6. Effect of Pressure (48 – 50 bar) on Adsorption of Histidine by Layered Hydroxide Minerals

In the study "Hydrothermal vents and the origin of life",[7] it was suggested that submarine volcanoes are places on the early Earth where the first prebiotic chemistry reactions might have occurred. Down in these underwater hotspots, the pressure would have been much higher than on the surface, due to the hydrostatic pressure of overlying seawater. Every 10-metre depth of seawater generates approximate 1 bar of pressure, and thus, there is a range of pressure between 200 – 400 bar in the depth between 2000 – 4000 m, changing the properties of the minerals, solutions, and reactions significantly. For this reason, the pressure factor must be considered when discussing prebiotic reactions in hydrothermal vents.

Kinetics of histidine adsorption by LDHs under high pressure have been investigated by Ikeda *et al.* in 1984.[56] In this survey, a relaxation method was used to produce an environment of sudden pressure jumps with a solution-containing chamber, a pressure pump, and a burst diaphragm made of 0.05 mm thick phosphor bronze. As the pump pressurised the chamber, reaching the limiting pressure (about 100 atm) of the membrane to rupture, an *in situ* electric conductivity detection and colorimetric ninhydrin dye-based methods were used to obtain the concentration changes of histidine in the solution. Results showed that there are kinetic differences between the intercalation rates of L- and D-histidine. The rate constant of intercalation-deintercalation of L-histidine was found to be larger than that of D-histidine.

Further related research was done on the effect of pressure on LDH intercalation of DNA strands, by Thyveetil *et al.*.[83] Through computer simulation, the

rise of pressure (up to 100 atm), together with temperature, was reported to increase the number of retained Waston-Crick hydrogen-bonded base pairs in the 108-base-pair DNA intercalated in a LDH interlayer, relative to the DNA in bulk water, showing an enhanced structural stability of DNA strands created by the LDH host.

6.1 Results and Discussion

Although each reacting vial was sealed with parafilm, and only a pin-prick was opened for the insertion of the conical condensation head, the solution level was found to be lower once the reactions at 30 °C, 50 bar were completed. In order to progress the research, and owing to the time constraints of the project period, this reaction was not re-run. Instead, the new liquid levels were marked below the levels before reaction. Some reacted solutions were then taken out for filtration before analysis, and the differences in solution level were carefully estimated by a syringe with needle. This factor of "concentration change" was entered into the calculation, in an attempt to reduce this systematic error.

Initial Concentration (M)	Volume loss (mL)	Factor in calculation
0.08	0.10	0.990
0.06	0.20	0.980
0.04	0.15	0.985
0.02	0.15	0.985
0.01	0.15	0.985
0.008	0.15	0.985
0.004	0.15	0.985

Table 8 The correction factor for vial fluid loss for reaction at 30 °C, 50 bar in calculation.

6.1.1 Adsorption isotherms at increased pressure

In the aspect of the adsorption isotherms, where the comparison of total absorbed amounts between different reaction conditions is considered and contrasted, there were some new observations being reported:

1. At a temperature of 30 °C, the LDH-Cl adsorbed less histidine at 50 bar than at ambient pressure.

2. The results were more complicated at 60 °C. In the concentrations above 0.02 M, LDH-Cl adsorbed more histidine at ambient pressure than at 48 bar, but less in the concentrations below 0.01 M.
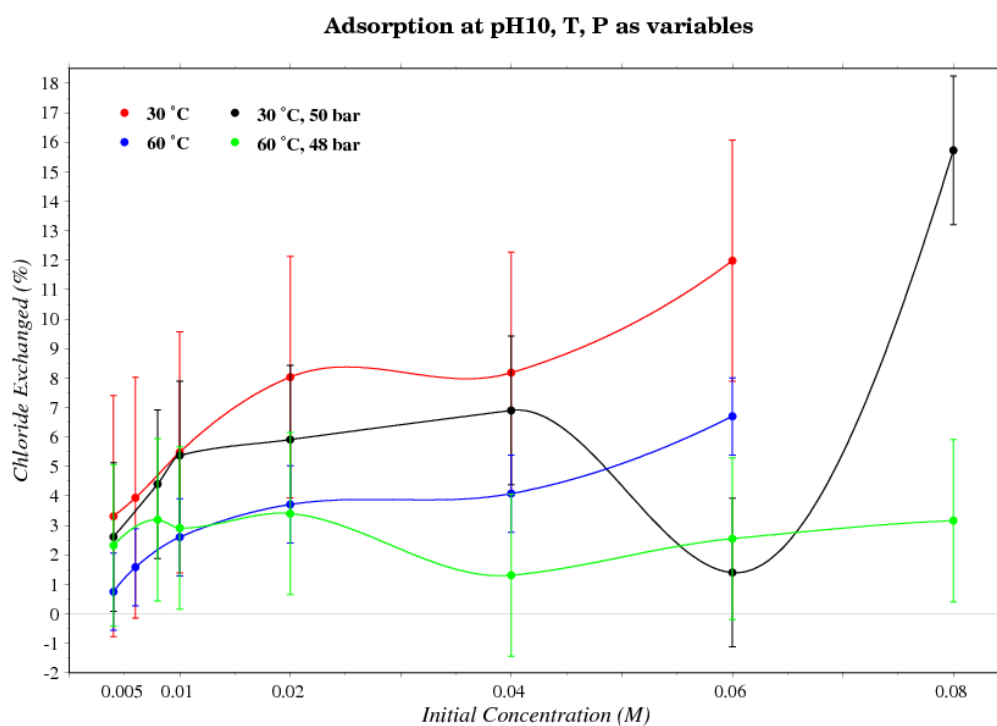
Figure 19 Comparison of adsorption isotherms of D, L-histidine at different T and P.

The reason for the observed trends was not immediately clear. It was postulated that the solvated histidine anion was surrounded by water molecules, with the high pressure effectively reducing the solvation distance. Therefore, higher activation energy may be needed for the histidine anion to be adsorbed to the surface of LDHs at the pressures about 50 bar. At higher temperatures, faster motion of molecules in solution increase the average distance of the histidine anion and water, reducing the solvation, but the effect was not obvious enough to reverse the trend between ambient and high pressure experiments until lowering the concentration of histidine anion. Diluting the histidine solution decreased the ionic strength, weakening the solvation between water and histidine further and thus exchanging more chloride out than in the experiments undertake at ambient pressure.

6.1.2 Chiral selectivity

In respect of "chiral selection", the L-histidine leads in the exchanging rate over the D-form under pressure. At 30 °C, 50 bar (see **Figure 18**), most of the differences were smaller than 0.1 %, except in two concentration: 1.86 % in 0.04 M and 0.67 % in 0.06 M. On the other hand, in the reaction at 60 °C, 48 bar (see **Figure 19**), the gap was growing larger with the concentration of histidine being diluted, from 0.2 % in 0.08 M to 1.38 % in 0.004 M. However, under 95 % confidence level, there were no significant differences between two enantiomers of intercalated histidine in both reactions, 30 °C, 50 bar and 60 °C, 48 bar.
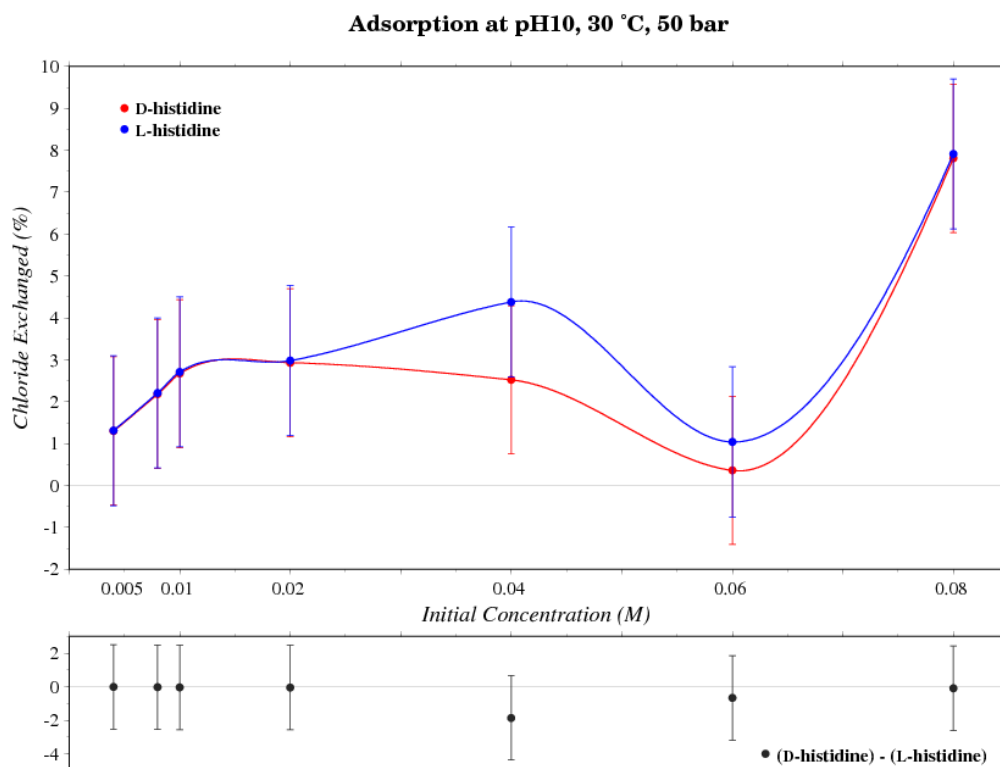
Figure 20   The percentage of interlayer chloride exchanged by D- and L-histidine at pH 10, 30 °C, 50 bar, and the differences between enantiomers (lower part). The error bar is the 95 % confidence interval (see Appendix for numbers) of each estimate.

Under these circumstances, it was postulated that there were no chiral selection in the intercalation of D, L-histidine into Mg_2Al-Cl LDH in both pressurised reaction conditions, 30 °C, 50 bar and 60 °C, 48 bar.

Compared to the kinetic study by Ikeda *et al.*, 1984,[56] that the rate of intercalation of L-histidine into Mg_2Al-Cl LDH was larger than D-form under pressure up to about 100 atm, the result here showed that there is no difference between the amounts of intercalated D- and L-histidine at equilibrium condition and the pressure about 50 bar.
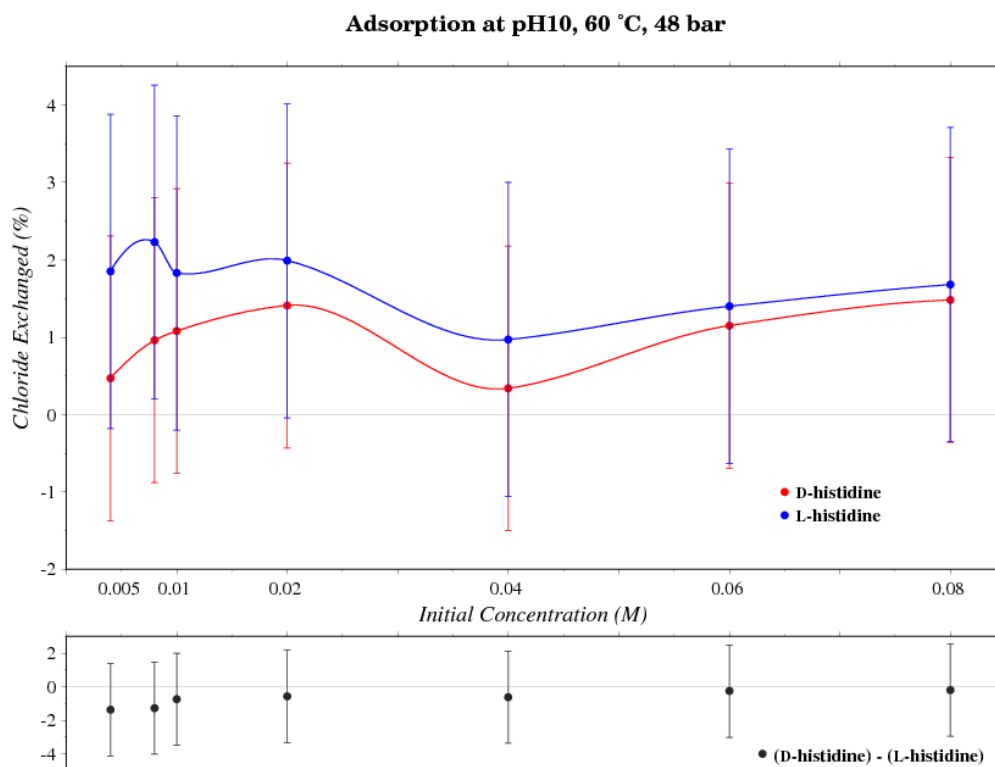
Figure 21   The percentage of interlayer chloride exchanged by D- and L-histidine at

pH 10, 60 °C, 48 bar, and the differences between enantiomers (lower part). The error

   bar is the 95 % confidence interval (see Appendix for numbers) of each estimate.

6.2   Geochemical Context of the Origin of Life

Considering the potential environments available for prebiotic chemistry on

the prebiotic Earth, pressures in the range of 48 – 50 bar may be found in the depth of

approximate 500 m under the seas. Under the pressures at these depths, adsorption

reactions at 30 °C obtained more LDH intercalated histidine at most concentrations,

making it the better condition in preserving a larger quantity of histidine than at the

temperature of 60 °C. On the other hand, in respect of chiral selectivity, there were no

obvious differences between intercalated D- and L-histidine at both 30 °C and 60 °C.

In this case, it was speculated that environments with condition of 30 °C, 50 bar

pressure fitted better with the environments during peptide formation on the prebiotic Earth.

In previous studies, hydrothermal vents were found in the depth of 2000 – 10000 metres under sea level,[82, 85] with the hydrostatic pressure ranging from 200 – 1000 bar. This offered us a target for future studies. What are the adsorption isotherms and the chiral selectivity of histidine by LDHs at pressures above 200 bar? With answers of questions such as this known, across the other biogenic amino acids, the possible origin of life on Earth is closer to being discovered.

7. Conclusions

The aim of this study was to discover the possible environmental conditions on early Earth that would have brought about the abiotic, geochemical reactions on the path to the biochemically catalysed reactions of life. Among all, attention was paid to the intercalation reaction of histidine, one of the essential amino acids, into layered double hydroxide, a possible mineral having involved in the formation of bio-active peptides, by direct ion exchange method.

The first stage was to prepare the LDH host mineral. Here, Mg_2Al-Cl LDH was successfully synthesised by co-precipitation method, and elemental analysis (CHN), ICP-OEC, TGA-MS, and PXRD were used for characterisation. There were five experiments involving synthesis, and three of there were used in the following adsorption experiments.

The second stage was the ion-exhange reactions of histidine into LDH-Cl, and conclusions were:

1. The experiment at pH 7, 30 °C was unsuccessful, for the histidine solutions were not prepared at pH 7, but around pH 4 depending on the concentrations. Three solutions below pH 4 were speculated to be unreacted, because Mg_2Al-LDH dissolved quickly under this condition. Histidine in the other three solutions of pH above 4 was exchanged through coupled anion with co-intercalated chlorides or carbonate, from partial dissolution of LDH-Cl powder.

2. The experiments at pH 10, 30 °C and 60 °C showed the same trends at

60

various concentrations, following the Langmuir model of adsorption isotherm,[72] basically, and the reaction at 30 °C intercalated more histidine into LDH-Cl than at 60 °C. Regarding chiral selection, the differences between the enantiomers were not significant enough to make any conclusions, at 30 °C or 60 °C, possible or meaningful.

3. In the pressurised experiments, 30 °C, 50 bar and 60 °C, 48 bar, the amounts of intercalated histidine anions were smaller than those under similar conditions but at ambient pressure, except in the solutions below 0.01 M at 60 °C, 48 bar. Both experiments showed no significant chiral selections, either.

Within these experimental conditions of ion-exchange reactions, the reaction at 30 °C, 50 bar, with the higher amounts of intercalated histidine for peptide formation in pressurised conditions, was considered to be the best case to fit the early Earth environmental conditions for the hypothesis of life having emerged at hydrothermal vents.

8. Further Work

After the completion of this study, there are still many issues worth investigation such as: improving the evidence of chiral selection; and experiments involving histidine intercalation at other temperature and pressure conditions.

None of the ion-exchange reactions in this study was able to be evidenced as showing chiral selectivity, owing to the small differences observed between the amounts of each enantiomer of intercalated histidine. In order to obtain more evidence about the chiral selection we are interested in, random error of analysis could be reduced through multiple measurements of each standard solution, and differences between enantiomers of intercalated histidine could be enhanced through larger quantities of LDH added in ion-exchange reactions.

Beyond the conditions used in the ion-exchange experiments, 30 °C and 60 °C at ambient pressure and pressure around 50 bar, there are still other conditions worth testing. According to previous studies,[7, 82, 85] hydrothermal vents that are possible origin of life were situated at depths of 2000 – 10000 m under sea level, supplying a hydrostatic pressure of 200 – 1000 bar, and the 100 °C, mineral-rich fluids were exhaled from hydrothermal vents to the 2 °C seawater, resulting a gradient of temperature of 100 °C to 2 °C. Reactions in various combinations of pressure and temperature may lead to different amounts of intercalation and different degrees of chiral selection, within which the best conditions for origin of homochirality may be found.

Appendix

	Standard deviation (%)			95 % confidence interval (%)		
	D-His	L-His	D+L, D−L	D-His	L-His	D+L, D−L
pH 7	1.96	2.08	2.85	3.83	4.07	5.59
pH 10, 30 °C	1.83	1.00	2.08	3.58	1.96	4.09
pH 10, 60 °C	0.43	0.51	0.67	0.84	1.00	1.31
pH 10, 30 °C, 50 bar	0.90	0.91	1.28	1.77	1.79	2.52
pH 10, 60 °C, 48 bar	0.94	1.04	1.40	1.84	2.04	2.57

Bibliography

1. D. E. Koshland, *Science*, 2002, **295**, 2215–2216.

2. J. D. Oliver and R. S. Perry, *Origins of Life and Evolution of Biospheres*, 2006, **36**, 515–521.

3. S.J. Mojzsis, G. Arrhenius, K. D. McKeegan, T. M. Harrison, A. P. Nutman and C. R. L. Friend, *Nature*, 1996, **384**, 55–59.

4. S. L. Miller, *Biochemica Et Biophysica Acta*, 1957, **23**, 480–489.

5. K. Plankensteiner, H. Reiner and B. M. Rode, *Current Organic Chemistry*, 2005, **9**, 1107–1114.

6. J. G. Blank, G. H. Miller, M. J. Ahrens and R. E. Winans, *Origins of Life and Evolution of Biospheres*, 2001, **31**,15–51.

7. W. Martin, J. Baross, D. Kelley and M. J. Russell, *Nature Reviews Microbiology*, 2008, **6**, 805–814.

8. A. P. Johnson, H. J. Cleaves, J. P. Dworkin, D. P. Glavin, A. Lazcano and J. L. Bada, *Science*, 2008, **322**, 404.

9. S. L. Miller, *Science*, 1953, **117**, 528–529.

10. S. L. Miller, H. C. Urey, *Science*, 1959, **130,** 245–251.

11. M. J. Russell and N. T. Arndt, *Biogeosciences*, 2005, **2**, 97–111.

12. G. Arrhenius, *Earth, Moon, and Planets*, 1987, **37**, 187–199.

13. K. Kruger, P. J. Grabowski, A. J. Zaug, J. Sands, D. E. Gottschling and T. R. Cech, *Cell*, 1982, **31**, 147–157.

14. T. R. Cech, *Science*, 1987, **236**, 1532–1539.

15. C. Guerrier-Takada, K. Gardiner, T. Marsh, N. Pace and S. Altman, *Cell*, 1983, **35**, 849–857.

16. W. H. McClain, C. Guerrier-Takada and S. Altman, *Science*, 1987, **238**, 527–530.

17. G. F. Joyce, *Gene*, 1989, **82**, 83–87.

18. G. F. Joyce, *Nature*, 1989, **338**, 217–224.

19. W. Gilbert, *Nature*, 1986, **319**, 618.

20. C. P. J. Maury, *Origins of Life and Evolution of Biospheres*, 2009, **39**, 141–150.

21. D. Voet, J. G. Voet and C. W. Pratt, *Fundamentals of Biochemistry: Life at the Molecular Level*, 3rd ed., Wiley, 2008

22. H. J. Cleaves, A. D. Aubrey and J. L. Bada, *Origins of Life and Evolution of Biospheres*, 2009, **39**, 109–126.

23. J. H. Jensen, K. K. Baldridge and M. S. Gordon, *Journal of Physical Chemistry*, 1992, **96**, 8340–8351.

24. A. Rimola, M. Sodupe and P. Ugliengo, *Journal of the American Chemical Society*, 2007, **129**, 8333–8344.

25. S. W. Fox and K. Harada, *Science*, 1958, **128**, 1214.

26. B. M. Rode, H. L. Son, Y. Suwannachot and J. Bujdák, *Origins of Life and Evolution of Biospheres*, 1999, **29**, 273–286.

27. H. L. Son, Y. Suwannachot, J. Bujdák and B. M. Rode, *Inorganica Chimica Acta*, 1998, **272**, 89–94.

28. L. Leman, L. Orgel and M. R. Ghadiri, *Science*, 2004, **306**, 283–286.

29. M. G. Schwendinger and B. M. Rode, *Analytical Sciences*, 1989, **5**, 411–414.

30. B. M. Rode and Y. Suwannachot, *Coordination Chemistry Reviews*, 1999, **192**, 1085–1099.

31. B. Chen, J. R. G. Evans, H. C. Greenwell, P. Boulet, P. V. Coveney, A. A. Bowden and A. Whiting, *Chemical Society Reviews*, 2008, **37**, 568–594.

32. L. E. Orgel, *Origins of Life and Evolution of Biospheres*, 1998, **28**, 227–234.

33. G. O. Arrhenius, *Helvetica Chimica Acta*, 2003, **86**, 1569–1586.

34. F. R. Costa, M. Saphiannikova, U. Wagenknecht and G. Heinrich, *Advances in Polymer Science*, 2008, **210**, 101–168.

35. M. Wei, M. Pu, J. Guo, J. B. Han, F. Li, J. He, D. G. Evans and X. Duan, *Chemistry of Materials*, 2008, **20**, 5169–5180.

36. D. G. Evans and R. C. T. Slade, *Structure and Bonding*, 2006, **119**, 1–87.

37. M. A. Ulibarri, M. J. Hernandez and J. Cornejo, *Journal of Material Science*, 1991, **26**, 1512–1516.

38. M. J. Kang, S. W. Rhee, H. Moon, V. Neck and T. Fanghanel, *Radiochimica Acta*, 1996, **75**, 169–173.

39. U. Constantino, M. Casciola, L. Massinelli, M. Nocchetti and R. Vivani, *Solid State Ionics*, 1997, **97**, 203–212.

40. S. Miyata and T. Kumura, *Chemistry Letters*, 1973, **2**, 843–848.

41. S. Miyata, *Clays and Clay Minerals*, 1983, **31**, 305–311.

42. D. S. Robins and P. K. Dutta, *Langmuir*, 1996, **12**, 402–408.

43. C. R. Gordijo, C. A. S. Barbosa, A. M. D. Ferreira, V. R. L. Contantino and D. D. O. Silva, *Journal of Pharmaceutical Sciences*, 2005, **94**, 1135–1148.

44. J. H. Choy, S. Y. Kwak, J. S. Park and Y. J. Jeong, *Journal of Material Chemistry*, 2001, **11**, 1671–1674.

45. M. C. Hermosin, I. Pavlovic, M. A. Ulibarri and J. Cornejo, *Journal of Environmental Science and Health A*, 1993, **28**, 1875–1888.

46. I. Soma, H. Wakano, H. Takahashi and M. Yamaguchi, Flame-Resistant Vinyl Chloride Resin Compositions. Jap. Patent 50,063,047, May 29, 1975.

47. M. Zammarano, F. Massimiliano, S. Bellayer, J. W. Gilman and S. Meriani, *Polymer*, 2005, **46**, 9314–9328.

48. J. R. Génin, R. Aïssa, A. Géhin, M. Abdelmoula, O. Benali, V. Ernstsen, G. Ona-Nguema, C. Upadhyay and C. Ruby, *Solid State Sciences*, 2005, **7**, 545–572 .

49. T. Hibino, *Chemistry of Materials*, 2004, **16**, 5482–5488.

50. D. G. Blackmond, *Cold Spring Harbor Perspectives in Biology*, 2010, **2**, a002147.

51. O. Botta, D. P. Glavin, G. Kminek and J. L. Bada, *Origins of Life and Evolution of Biospheres*, 2002, **32**, 143–163.

52. D. G. Fraser, H. C. Greenwell, N. T. Skipper, M. V. Smalley, M. A. Wilkinson, B. Demé and R. K. Heenan, *Physical Chemistry Chemical Physics*, 2011, **13**, 825–830.

53. J. Bujdák, M. Remko and B. M. Rode, *Journal of Colloid and Interface Science*, 2006, **294**, 304–308.

54. T. Shibata, J. Yamamoto, N. Matsumoto, S. Yonekubo, S. Osanai and K. Soai, *Jounal of the American Chemical Society*, 1998, **120**, 12157–12158.

55. D. Fitz, H. Reiner, K. Plankensteiner and B. M. Rode, *Current Chemcial Biology*, 2007, **1**, 41–52.

56. T. Ikeda, H. Amoh and T. Yasunaga, *Jounal of the American Chemical Society*, 1984, **106**, 5772–5775.

57. J. A. D. Wattis and P. V. Coveney, *Origin of Life and Evolution of Biospheres*, 2005, **35**, 243–273.

58. S. I. Goldberg, *Origin of Life and Evolution of Biospheres*, 2007, **37**, 55–60.

59. F. Li, D. Fitz, D. G. Fraser, B. M. Rode, *Amino Acids*, 2010, **38**, 287–294.

60. S. Miyata, *Clays and Clay Minerals*, 1975, **23**, 369–375.

61. Q. Yuan, M. Wei, D. G. Evans and X. Duan, *Journal of Physical Chemistry B*, 2004, **108**, 12381–12387.

62. P. Porta and S. Morpurgo, *Applied Clay Science*, 1995, **10**, 31–44.

63. M. Wei, Q. Yuan, D. G. Evans, Z. Q. Wang and X. Duan, *Journal of Materials Chemistry*, 2005, **15**, 1197–1203.

64. E. L. Crepaldi, P. C. Pavan and J. B. Valim, *Jounal of Brazilian Chemical Society*, 2000, **11**, 64–70.

65. J. He, M. Wei, B. Li, Y. Kang, D. G. Evans, X. Duan, *Structure and Bonding*, 2006, **119**, 89–119.

66. M. A. Aramendia, V. Borau, C. Jiménez, J. M. Marinas, J. R. Ruiz and F. J. Urbano, *Journal of Solid State Chemistry*, 2002, **168**, 156–161.

67. Y. Zhao, F. Li, R. Zhang, D. G. Evans and X. Duan, *Chemistry of Materials*, 2002, **14**, 4286–4291.

68. István Pálinkó, *Nanopages*, 2006, **1**, 295–314.

69. J. W. Boclair and P. S. Braterman, *Chemistry of Materials*, 1999, **11**, 298–302.

70. D. C. Harris, *Quantitative Chemical Analysis*, 6th ed., New York: W. H. Freeman and Co., 2003

71. S. Aisawa, S. Sasaki, S. Takahashi, H. Hirahara, H. Nakayama and E. Narita, *Journal of Physics and Chemistry of Solids*, 2006, **67**, 920–925.

72. I. Langmuir, *Journal of the American Chemical Society*, 1916, **38**, 2221–2295.

73. D. R. Hines and S. A. Solin, *Physical Review B*, 2000, **61**, 11348–11358.

74. C. Vaysse, L. Guerlou-Demourgues, A. Demourgues, F. Lazartigues, D. Fertier and C. Delmas, *Journal of Materials Chemistry*, 2002, **12**, 1035–1043.

75. M. Ogawa and S. Asai, *Chemistry of Materials*, 2000, **12**, 3253–3255.

76. F. Kooli, I. C. Chisem, M. Vucelic and W. Jones, *Chemistry of Materials*, 1996, **8**, 1969–1977.

77. B. Lotsch, F. Millange, R. I. Walton and D. O'Hare, *Solid State Sciences*, 2001, **8**, 883–886.

78. W. Müller-Warmuth and R. Schöllhorn, *Progress in Intercalation Research*, Kluwer Academic, 1994, 1–514.

79. G. R. Williams, A. M. Fogg, J. Sloan, C. Taviot-Guéhod and D. O'Hare, *Dalton Transactions*, 2007, 3499–3506.

80. M. Thyveetil, P. V. Coveney, H. C. Greenwell and J. L. Suter, *Jounal of the American Chemical Society*, 2008, **130**, 12485–12495.

81. G. R. Williams, A. I. Khan, D. O'Hare, *Structure and Bonding*, 2006, **119**, 161–192.

82. M. J. Russell, *Science*, 2003, **302**, 580.

83. M. Thyveetil, P. V. Coveney, H. C. Greenwell and J. L. Suter, *Jounal of the American Chemical Society*, 2008, **130**, 4742–4756.

84. D. G. Fraser, D. Fitz, T. Jakschitz and B. M. Rode, *Physical Chemistry Chemical Physics*, 2011, **13**, 831–838.

85. H. W. Jannasch and M. J. Mottl, *Science*, 1985, **229**, 717–725.